The 2021 and 2022 North Coast California Earthquake Sequences and Fault Complexity in the Vicinity of the Mendocino Triple Junction

Margaret Hellweg*[1], Douglas S. Dreger[1], Anthony Lomax[2], Robert C. McPherson[3], and Lori Dengler[3]

ABSTRACT

The Mendocino Triple Junction (MTJ), one of the most tectonically active and complex regions of California, has damaging earthquakes on the San Andreas and Mendocino faults, within the oceanic and subducting regions of the Gorda section of the Juan de Fuca plate, and within the overriding North American plate (NAP). Two recent earthquake sequences in the MTJ region, starting on 20 December 2021 and 20 December 2022, highlight the complex interactions of regional faults. We explore these sequences to better define the deep faults in the MTJ region, and their rupture modes. Our finite-source analysis shows the 2021
2 **sequence began with two M ~6.0 earthquakes separated by ~11 s in time and 30 km in distance. The first earthquake occurred offshore on the Mendocino fault at a depth of 16.5 km. Its *S* waves triggered an "onshore" intraplate Gorda event at a depth of 27 km, which ruptured a vertical fault toward the northeast. Finite-source analysis of the mainshock of the 2022 sequence, M 6.4, indicates the rupture started offshore north of Cape Mendocino within the Gorda plate and propagated east-northeast, toward populated areas. Damage to towns and infrastructure was exacerbated by directivity and the sediment-filled valleys, as well as by a large aftershock (M 5.4) centered 20 km south-southeast of the mainshock rupture plane. The depths and mechanisms of the onshore 2021 and the 2022 earthquakes and their aftershock sequences indicate that they occurred on different strike-slip faults within the subducted portion of the Gorda plate. The faults active in these earthquakes are unrelated to mapped surface faults in the overriding NAP and are oblique to the tectonic trends seen at the surface. The 2021 and 2022 earthquakes are close to the boundary between two distinct regions of the Gorda plate, where offshore north–south horizontal compression transitions to east–west downslab tension.**

KEY POINTS

- We use large 2021 and 2022 earthquakes to better understand Mendocino Triple Junction tectonics and faulting.
- The earthquake fault orientations are consistent with north–south compression in the offshore Gorda plate.
- Seismotectonics in the Cape Mendocino area is complex with frequent interactions between earthquake ruptures.

Supplemental Material

INTRODUCTION

The Mendocino Triple Junction (MTJ) region, one of California's tectonically most active and complex regions, lies to the north of 40° N and west of 124° W (Fig. 1). Pioneering oceanic voyages in the 1950s (Raff and Mason, 1961) discovered and mapped a pattern of magnetic anomalies in the MTJ region forming a ridge-transform-trench configuration that defined the small, young oceanic plate that is subducting beneath northernmost California (Raff and Mason, 1961; Silver, 1969, 1971; Atwater, 1970). This small plate, which makes up the southernmost portion of the Cascadia Subduction Zone, has been called the Gorda plate, after the Gorda basin, named by Portuguese settlers who found fishing to be "fatter" in shallower waters in this area than further south. In early mapping, the magnetic anomalies in the southern part of the Gorda plate appeared distorted which was interpreted as a sign of internal deformation (Raff and Mason, 1961; Emilia *et al.*, 1968; Riddihough, 1980) and led researchers

1. Berkeley Seismology Laboratory, University of California Berkeley (retired), Orinda, California, U.S.A., https://orcid.org/0000-0002-6590-3089 (DSD); 2. Alomax Scientific Software, https://orcid.org/0000-0002-7747-5990 (AL); 3. California 1
Polytechnic Humboldt (retired), Arcata, California, U.S.A.

*Corresponding author: hellweg@berkeley.edu

Cite this article as Hellweg, M., D. S. Dreger, A. Lomax, R. C. McPherson, and L. Dengler (2024). The 2021 and 2022 North Coast California Earthquake Sequences and Fault Complexity in the Vicinity of the Mendocino Triple Junction, *Bull. Seismol. Soc. Am.* **XX**, 1–23, doi: 10.1785/0120240023

to divide the plate into northern and southern domains. The northern section, which moves in concert with the Juan de Fuca plate to its north, is relatively undeformed with its bathymetric fabric parallel to the ridge, (Riddihough, 1980, 1984; Wilson, 1986, 1989; Dziak *et al.*, 2001; Chaytor *et al.*, 2004). The southern portion is clearly deformed, its magnetic anomalies rotated clockwise away from the original ridge parallel alignment
3 (Atwater *et al.*, 1968; Wilson, 2002). Large earthquakes are a relatively frequent occurrence in the Gorda plate with events of $M_w \geq 6$ and depths on the order of 25 km occurring on average every five years in the past century (Dengler *et al.*, 1992; Bakun, 2000). Based on mechanisms, aftershock alignments and finite-source estimates, many of the offshore earthquakes exhibit left-lateral, strike-slip motion on northeast–southwest-trending vertical faults (Cockerham, 1984; Cockerham *et al.*, 1989; Smith *et al.*, 1993; Velasco *et al.*, 1994; Braunmiller *et al.*, 1997; Rollins and Stein, 2010; Guilhem and Dreger, 2011; Wei and McGuire, 2014) that parallel the trends of the rotated anomalies
4 (Gullick *et al.*, 1997; Dziak *et al.*, 2001; Wilson, 2002; Chaytor *et al.*, 2004).

Denlinger (1992) proposed that the offshore surface area of the Gorda plate is reduced by 25%–30% because it moves eastward through a tectonic constriction before descending beneath the North American plate (NAP). This is a consequence of the south-eastward movement of the Juan de Fuca plate relative to the Pacific plate (PP), which compresses the Gorda plate against the unyielding vertical barrier of the PP along the Mendocino fault (McPherson, 1989; Smith *et al.*, 1993; Wang *et al.*, 1997). The result is north–south directed horizontal compression in the offshore portion of the Gorda plate, the area west of the northeastern corner of the PP (see PP in Fig. 1, Prentice *et al.*, 1999; Hole *et al.*, 2000; Beeson *et al.*, 2017) at the east end of the Mendocino fault. This movement entails that large parts of the southern Gorda plate have undergone intense internal deformation, with rotated magnetic anomalies, large folds, and numerous historic vertical strike-slip, intraplate events (Velasco *et al.*, 1994; Dziak *et al.*, 2001; Chaytor *et al.*, 2004). Once the Gorda plate has passed the northeastern corner of the PP (Fig. 1), the north–south compression eases and the intraslab stress tensor indicates downslab directed east–west tension. Earthquake focal mechanisms change from vertical strike slip in the offshore zone to north–south normal mechanisms in the downgoing slab beneath the NAP (Cockerham, 1984, 1989; McPherson, 1989; Smith *et al.*, 1993; Wada *et al.*, 2010). For clarity, the reference to the corner of the PP is a seismic one. That is, we define the corner of the PP as the intersection of the projection of the 1906 rupture plane along the San Andreas fault with the relocated east–west trend of the Mendocino fault (Prentice *et al.*, 1999; Hole *et al.*, 2000; Beeson *et al.*, 2017; Lomax and Henry, 2023).

In this article, we focus on two earthquake sequences in the MTJ region that occurred one year apart in December 2021 and December 2022. These two sequences are near the corner of the PP (Fig. 1) where stress regimes undergo a transition. They offer an opportunity to further investigate the faults in the region and their modes of rupture. It is important that we will use the alignment of the stress tensor in the region of the MTJ as an indicator identifying which plate an earthquake is in, with each plate in the MTJ region exhibiting a distinct orientation (McPherson, 1989; Smith *et al.*, 1993). As described earlier, the offshore region of the Gorda plate is defined by north–south horizontal compression and hosts vertical strike-slip faults. To the east, where the Gorda plate has extruded past the corner of the PP (Fig. 1), the stress regime exhibits down-slab "tension" and north–south-oriented normal faulting with smaller magnitude earthquakes (Cockerham *et al.*, 1989; Smith *et al.*, 1993; Wada *et al.*, 2010). This change in focal mechanisms suggests that within the downslab region faulting is presently cross cutting the fabric of the Gorda plate, whereas offshore faulting parallels the fabric.

To assess the orientation of current stresses within the NAP above the subduction interface, we use the results of an analysis of 44 well-located NAP earthquakes which occurred between 1974 and 1986 during the deployment of the Humboldt Bay Seismic Network (McPherson, 1989; Smith *et al.*, 1993). Seismicity in the NAP was determined to be dominated by reverse mechanisms consistent with the mapped active surface faults (Ogle, 1953; Kelsey and Carver, 1988; Clarke and Carver, 1992; McLaughlin *et al.*, 2000). The P axes are horizontal, ranging from north–south to N70°E. The T axes are primarily vertical, although some are low angle (McPherson, 1989; Smith *et al.*, 1993). The orientations of the P and T axes are consistent with east–west to northeast–southwest reverse faulting with additional right lateral strike-slip faulting, in agreement with the Holocene surface faults and folds (Kelsey and Carver, 1988; McPherson, 1989; Clarke and Carver, 1992). Just as the Gorda plate is divided into two regions based on intraplate stress orientations, the NAP incurs dramatic internal changes in stress as one moves from south to north past the corner of the PP (Fig. 1). South of the Mendocino fault, which defines the northern extent of the PP, the NAP exhibits stress tensor alignment, and the Global Navigation Satellite System (GNSS) vectors, consistent with a broad northwest–southeast-trending strike-slip boundary (Williams *et al.*, 2006; McKenzie and Furlong, 2021; Nuyen and Schmidt, 2022; Materna *et al.*, 2023). North of the Mendocino fault, the GNSS vectors rotate into a very different subduction-influenced environment. Both the stress tensor alignment and the fabric of the surface geology within the NAP is distinct from that of the Gorda plate below. The observations of these distinct differences in the conditions of the interacting plates in the MTJ are also important to understanding the details of the 2021 and 2022 earthquake sequences described in this article (Ogle, 1953; Smith *et al.*, 1993; Gullick *et al.*, 1998, 2001; Williams *et al.*, 2006; McKenzie and Furlong, 2021; Nuyen and Schmidt, 2022).

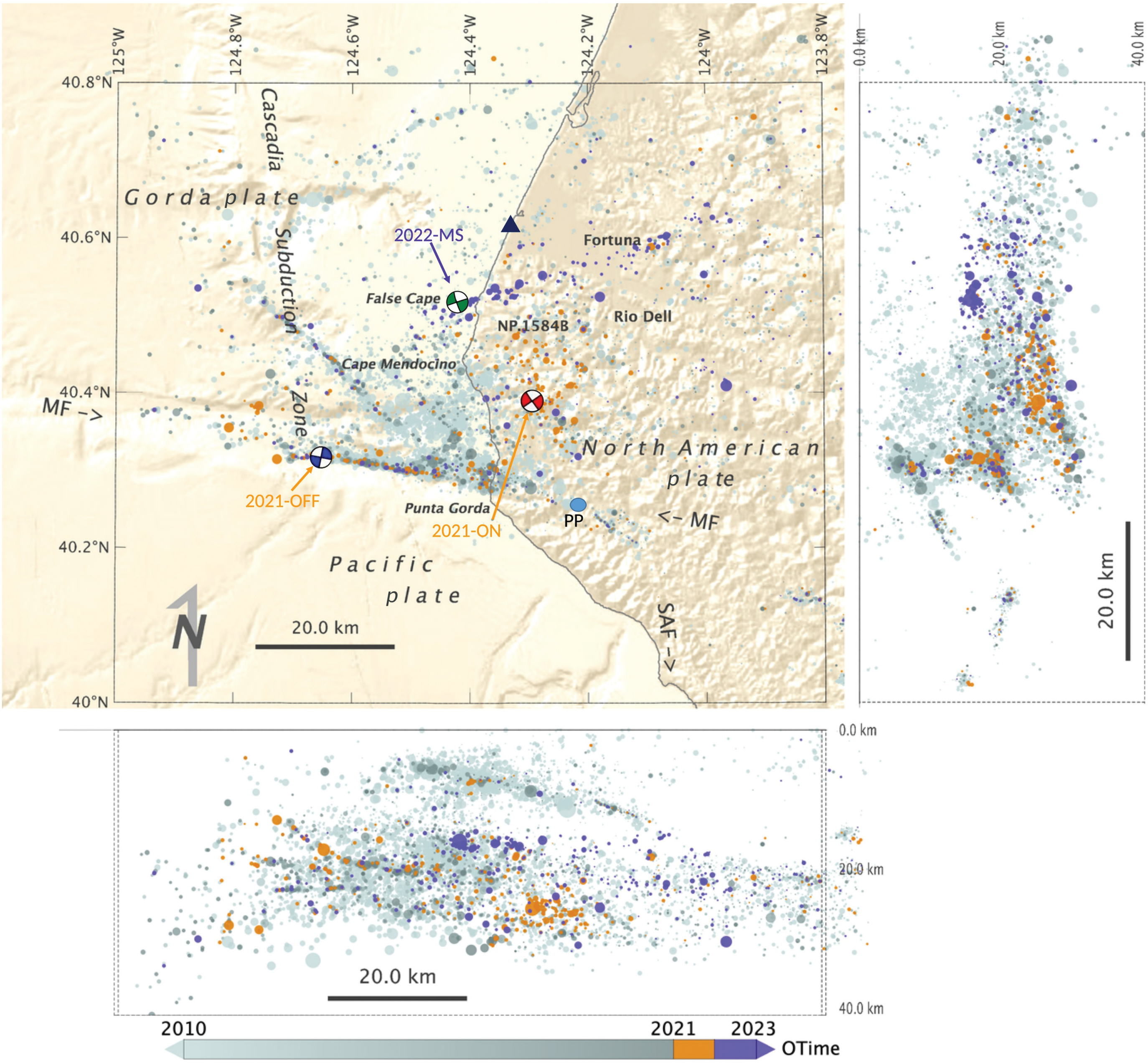

Figure 1. Seismicity from the region of the Mendocino Triple Junction (MTJ) from 1982 to 2023 taken from the catalog of the Northern California seismic system (see Data and Resources) and relocated using the NLL-SSST-Coherence (NLL-SC; Lomax and Savvaidis, 2022; Text S1). The complete relocated catalog is included as supplemental File S1, with a movie of this plot viewed from a variety of angles included as supplemental Movie S1 (see Data and Resources). Seismicity is shown in the map view (center), including topography and bathymetry from the National Oceanic and Atmospheric Administration (NOAA) (Data and Resources), as well as depth cross-sections viewed from the south (bottom) and east (right). Shades of gray indicate epicenters of earthquakes between 1982 and 20 December 2021. Orange circles are earthquakes between 20 December 2021 and 20 December 2022. Blue circles are earthquakes that occurred from 20 December 2022 to 10 October 2023. Mechanisms are shown for the three earthquakes analyzed in this article, 2021-OFF (blue), 2021-ON (red), and 2022-MS (green). All orange and blue events are within the band of intraplate events defining the Gorda plate. MF, Mendocino fault; SAF, San Andreas fault. The light blue dot indicates the location of the corner of the Pacific plate (PP) and the black triangle indicates the Fleener Creek block slide shown in Figure 10. 26

Another important consideration in understanding the rupture history of the 2021 and 2022 sequences is the geometry of the subduction zone in the hypocentral region of each rupture. Estimates of the position of the top of the Gorda plate have evolved over time. McCrory *et al.* (2012) made one of the first comprehensive attempts to contour the top of the Gorda slab as part of the slab 1 model for the entire Cascadia subduction zone. In the hypocentral regions of the two offshore events in the present study, we find, as do Gong and McGuire (2021), that the shallower slab 2 contours (Hayes *et al.*, 2018) better fit our findings than do the slab 1 contours defined by McCrory *et al.* (2012).

Determining the depth to the Gorda interface in the vicinity of the MTJ is challenging. Offshore of the MTJ region, seismic lines image the top of the Gorda crust at slightly less than 5 km

5 west of the accretionary wedge (Gullick *et al.*, 1998; Gullick, 2001). These seismic lines agree well with the intraslab earthquake locations we present here, as well as with older interpretations (McPherson, 1989; Lomax and Henry, 2023, supplemental data). To the east in the regions just offshore, the position of the top of the Gorda plate becomes less certain. We consulted a variety of studies, including an onshore 140-
6 km-long refraction/reflection study (Beaudoin *et al.*, 1994), offshore seismic studies (Gullick *et al.*, 1998; Carbotte *et al.*, 2024), V_P/V_S estimates (Guo *et al.*, 2018), converted phases (Gong and McGuire, 2021), receiver functions (Delph *et al.*, 2021; Bloch *et al.*, 2023), and other studies of these two earthquake sequences (Yeck *et al.*, 2023; Shelly *et al.*, 2024; Yoon and Shelly, 2024). All these independent investigations agree that the Wadati–Benioff (Gorda intraslab) earthquakes are at or below their postulated megathrust boundaries. Thus, we infer the position of the plate or plates in which each rupture occurs on the relocations of the seismicity in the region described here and on the orientation of the stress tensor determined from the mechanism of each mainshock. In all cases, this inference is consistent with the positions of the top of the Gorda plate described in the previously mentioned studies.

Over the past 5 yr, improvements in the seismic and deformation monitoring infrastructure in the region around the MTJ have been implemented as part of the development and deployment of the ShakeAlert earthquake early warning system along the United States (US) West Coast (Given *et al.*, 2018). Both the 2021 and 2022 event sequences triggered ShakeAlert (see Data and Resources).

The high-dynamic range data from modern seismic instrumentation and the continuous data from the GNSS receivers offer an opportunity to investigate the “20 December” earthquakes of 2021 and 2022 and their aftershocks in greater detail.

The Berkeley Seismology Laboratory (BSL) has developed a number of tools to improve the understanding of local and regional earthquakes, including time-domain determination of moment tensors (tdmt) using full waveforms (e.g., Pasyanos *et al.*, 1996; Dreger, 2003, 2018); real-time grid searches for earthquake source location, mechanism and magnitude, for example, GridMT (Guilhem and Dreger, 2011); and finite-source analysis of strong (M ≥6) earthquakes (Kaverina *et al.*, 2002; Dreger *et al.*, 2015). We apply these methods, as well as
7 multiscale precise event relocation using NLL-SSST-Coherence (NLL-SC; Lomax and Savvaidis, 2022, see Text S1, available in the supplemental material to this article), to explore these two earthquake sequences which occurred one year apart. The complete NLL-SC relocated catalog is included in supplemental File S1 (see Data and Resources).

THE DECEMBER 2021 AND 2022 EARTHQUAKES

Earthquakes in the MTJ region on 20 December 2021 at 20:10:20 UTC (12:10:20 PST) were widely felt but caused only minor damage. The earthquake on 20 December 2022 at 10:34:20 UTC (02:34:24 PST) caused major damage to the city of Rio Dell and moderate damage elsewhere in southern Humboldt County (Fig. 1, Table 1). Additional damage in the area was caused by the 18:35:04 UTC M 5.4 aftershock about 20 km south-southeast of the main rupture on 1 January 2023.

The 20 December 2021 events were initially reported as a single M 6.2 earthquake occurring 30 km offshore of Cape Mendocino along the Mendocino fault. Most people also perceived the earthquakes as a single event, although aftershocks formed two clearly separated clusters of events over the course of the following days (Fig. 1, orange dots). The “Did You Feel It?” Community Internet Intensity map (Atkinson and Wald, 2007) exhibits averaged intensities of 6–7 in the epicentral area near Cape Mendocino. The peak acceleration of 33%*g* was recorded at Petrolia, and the earthquakes resulted in little damage. No significant damage was reported to roads, bridges, or other public structures, and no local or state emergency declarations were made.

One year later, on 20 December 2022, the local population was jolted awake shortly after 02:34:24 PST (10:34:34 UTC, Table 1) by an M 6.4 earthquake. Two of the authors (L. D. and R. C. M.) received reports from many people in this earthquake-prone region that the event produced the strongest shaking they had ever felt. Two strong-motion instruments in Rio Dell about 10 km from the fault recorded peak accelerations above 1*g*. The highest acceleration was 1.44*g* at station CE.89462, operated by the California Geological Survey (CGS) at the Rio Dell-101/Painter Street Overpass Grounds (see Data and Resources). Considering the frequent occurrence of moderate-to-large earthquakes in the region, the shaking produced unexpectedly large damage in both old and new buildings and infrastructure. According to Humboldt County Office of Emergency Services (2023), it caused at least $32 million U.S. in property losses, whereas a more recent study focused on lifeline losses puts Rio Dell losses at $92 million U.S. (J. Eidinger, personal comm., 2024). Nearly a quarter of the residents of Rio Dell were displaced due to damage to residences. Two people died due to medical-related conditions and 17 injuries were reported. California declared a State of Emergency.

The epicenter of this event was just offshore of False Cape, to the north of Cape Mendocino (Fig. 1, blue dots). Its aftershocks stretch from the epicenter to the east-northeast for about 50 km, a relatively long distance for an M 6.4 event, with scattered aftershocks radiating out further toward the east and northeast. The 2022 event appears to have reruptured the same fault that hosted the 7 June 1975, Rio Dell earthquake and caused similar patterns of damage in the region (McPherson *et al.*, 2023, 2024). Thus, we consider it to be a large repeating earthquake. The largest aftershock of the 2022 earthquake occurred on 1 January 2023, to the south-southeast of the fault, well off the main trend of seismicity. It ruptured northwest toward Rio Dell causing additional damage to houses and infrastructure there, as well

TABLE 1
Origin Information about the 2021 Doublet Earthquakes (Offshore and Onshore), the 2022 Mainshock, and Its Major Aftershock (1 January 2023)

							Closest Station†		Highest PGA†	
29 Earthquake	Source (Hypocenter/ Magnitude)*	Origin Time (UTC) (yyyy/ mm/dd hh: mm:ss.ss)	Latitude (°N)	Longitude (°W)	Depth (km)	Magnitude	Station Location of PGA†	PGA, Epicentral Distance	Station Location of PGA†	PGA, Epicentral Distance
2021-OFF	NCSS/NCSS	2021/12/20 20:10:20.31	40.298	124.626	16.5	5.65 M_L	–	–	–	–
	NLL/This article‡	2021/12/20 20:10:20.31	40.315	124.647	17.2	6.02 M_w				
2021-ON	NCSS/NCSS	2021/12/20 20:10:31.31	40.390	124.298	27.0	6.2 M_w	CE.89005 Cape Mendocino	0.17*g*, 6.6 km	CE.89462 Rio Dell	0.444*g*, 20.9 km
	NLL‡/This article	2021/12/20 20:10:31.24	40.389	124.294	25.7	6.06 M_w				
2022-MS	NCSS/ NCSS	2022/12/20 10:34:24.77	40.525	124.423	17.9	6.4 M_w	NC.KCT Cape Town	0.12*g*, 9.1 km	CE.89462 Rio Dell	1.46*g*, 27.4 km
	NLL‡/This article	2022/12/20 00:34:24.77	40.389	124.294	25.7	6.45 M_w				

NCSS, Northern California Seismic System; PGA, peak ground acceleration.
*For hypocenter and magnitude sources, see Data and Resources.
†For strong-motion station information and parameter sources, see Data and Resources.
‡For a description of the NLL processing and procedures, see the supplemental material.

as minor cliff failure along the nearby Scotia Bluffs on the Eel River (R. C. M., see Data and Resources).

DECEMBER 2021 EARTHQUAKE SEQUENCE

For several weeks after it occurred, the earthquake on 20 December 2021 was listed in the Northern California Seismic System (NCSS) catalog as having a magnitude of M 6.2 and an epicenter on the Mendocino fault around 30 km offshore. In addition to the two clearly separated clusters of aftershocks, one tracking the lineament of the Mendocino fault and the second appearing spatially more diffuse on the map and under the NAP (Fig. 1), other observations also suggested that the earthquake source might be more complex. These included the shaking recorded and reported on land, the phase arrivals recorded at seismograms from onshore stations and the mechanism determined through moment tensor analysis. The accelerometer station NP.1584 lies near the center of the second aftershock cluster. The recording from this station provides a clearer view of what happened (Fig. 2). On the vertical channel at this site, a *P*-wave arrives at 20:10:27.86 UTC. A short time later a second *P*-wave arrives, at 20:10:36.5 UTC. On the horizontal channels, *S* arrivals are apparent at 20:10:33.9 UTC and 20:10:40.6 UTC. Clear picks for both the *P* and *S* waves at this station and others nearby allowed the determination of locations for two separate earthquakes.

It was a challenge to disentangle the waveforms of the two earthquakes at many stations because unlike many "doublets" that occur within a few seconds of each other, these two were not in the same location, and the second, onshore event nucleated at about the time that waves from the first earthquake arrived at its location. Thus, waves from the two earthquakes are superimposed at stations outside of the epicentral region (see Data and Resources). The first earthquake (2021-OFF) occurred offshore along the Mendocino fault at 20:10:20.31 UTC; the second earthquake (2021-ON) followed 11 s later at 20:10:31.31 UTC under the continental, NAP, or "onshore" (Table 1, Fig. 1).

Determining the magnitudes of the two earthquakes is also difficult. No coda magnitude (Eaton, 1992) can be determined for 2021-OFF because its coda is fully subsumed in the second earthquake. The second earthquake, 2021-ON, appears larger because its epicenter is closer to recording stations. Because of the overlapping waveforms, any moment magnitude determined from full waveforms would be associated with the later event. Staff of the Bay Area Earthquake Monitoring Project (EMP) of the U.S. Geological Survey (USGS) determined a local magnitude of M_L 5.7 for 2021-OFF (Richter, 1935; Uhrhammer *et al.*, 2011) using the *S*-wave amplitudes measured at the stations closest to the coast, where they were uncorrupted by 2021-ON (H. MacBeth, personal comm., 2022). A regional moment tensor (Dreger, 2018) was determined for 2021-ON, once its hypocenter had been determined, giving it a magnitude of M_w 6.2 (see Data and Resources).

December 2021 GridMT application

Although it was not running in real time when the earthquakes occurred, a GridMT algorithm had previously been developed

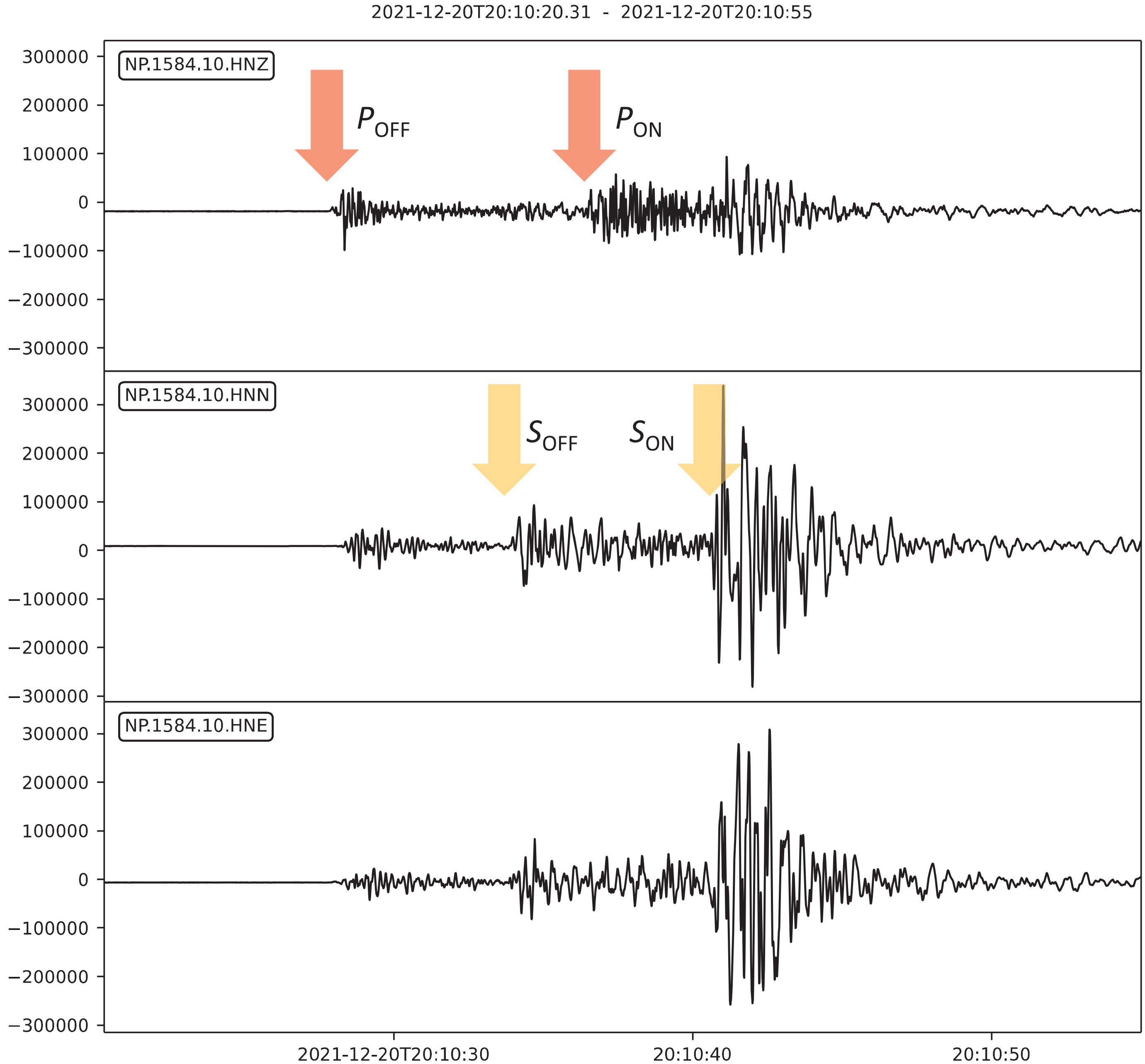

Figure 2. Waveforms from station NP.1584 (see Data and Resources) starting at the origin time of 2021-OFF. Units of the vertical axes are counted. Light gray arrows mark the *P*-wave arrivals for the two events of the doublet, whereas dark gray arrows mark the *S*-wave arrivals at this station.

for the region (Guilhem and Dreger, 2011). The GridMT method (Tsuruoka *et al.*, 2009) makes use of a continuous stream of waveform data to simultaneously detect earthquakes, locate them and determine their seismic moment tensors and moment magnitudes. When implemented automatically, the method provides an autonomous seismic monitoring workflow. For the December 2021 events, we applied the GridMT approach to the recorded broadband displacement waveforms to try to determine an improved location and seismic moment tensor solution for the primary moment release. An 80 × 80 km grid with 5 km horizontal spacing provided 256 virtual source locations (Fig. 3) for each source depth. Depth slices at 16, 18, 20, 22, 24, 27, 30, 33, and 36 km were tested, giving a total of 2304 possible source locations at which moment tensors were determined. The GIL7 velocity model (Dreger and Romanowicz, 1994) was used to compute Green functions using the CPS3.0 frequency–wavenumber (*f*-*k*) integration program (Herrmann, 2013). Figure 3 shows the GridMT result indicating that at long periods (50–20 s) of the primary moment release takes place approximately 30–40 km northeast of the offshore hypocenter located on the Mendocino fault. The grid search indicates that the event is deep as the fit steadily increases with depth, although the fit curve flattens at depths greater than 30 km. Therefore, we choose 30 km as the best

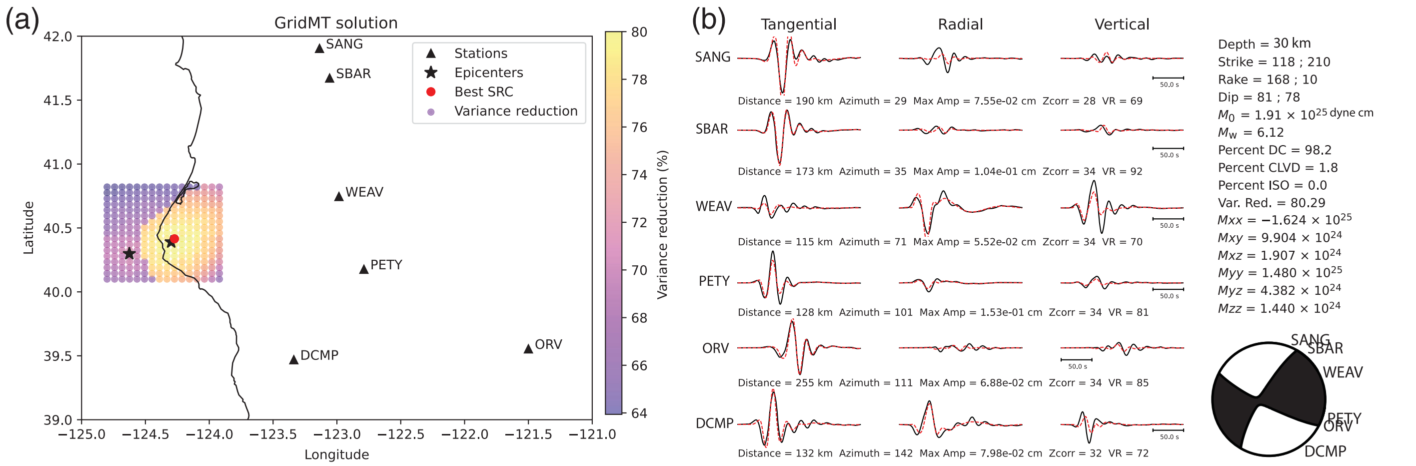

Figure 3. (a) Grid of virtual sources (circles) at 30 km depth color coded by fit 27 (variance reduction, %) to the long-period displacement waveform data for the December 2021 event. The best-fit source is the red circle. Black stars show the epicentral locations (Table 1) of the doublet. (b) Moment tensor product from the location with the best fit from GridMT (40.415° N, 124.272° W, and 30 km depth) for 2021-ON. Displacement data and synthetics are band-pass filtered between 50 and 20 s period using an acausal Butterworth filter.

depth from the inversion (Fig. 3a), placing the event well below the top of the subducted Gorda plate. The 50–20 s period waveform fits shown in Figure 3b are quite good for the main moment release at the onshore location. Although the stations are all located to the east of the event, the moment tensor is well constrained and indicates nearly pure strike slip on northeast- or southeast-striking planes. The GridMT application successfully locates the main moment release, estimates M_w 6.1 for the event, and at long periods, the single centroid location fits well. However, the raw waveforms in Figure 2 show that the event is indeed two earthquakes separated by a short-time interval. To model the short-period waveforms, a distributed finite-source approach is needed to unravel the faulting complexity.

December 2021 finite-source inversion

We applied a method for determining finite sources for regional events developed at the BSL (Kaverina *et al.*, 2002) to this complex earthquake doublet. This method is a multiple
8 time-window approach based on Hartzell and Heaton (1982) and can invert seismic waveform data, GNSS displacements, and the Interferometric Synthetic Aperture Radar (InSAR) derived deformation. We began with a multiple time-window parameterization. However, we found that the multiple time windows were not well resolved and over parameterized the model as the earthquakes' magnitudes are near the lower limit of the method's capabilities given the relatively poor station coverage. Therefore, we simplified the model by considering only a single time window, effectively limiting the rise time and requiring the rupture velocity to be constant. Broadband data from a suite of regional stations (BK.JCC, BK.SIGP, BK.SCOT, BK.PETY, and BK.WEAV) were used, as well as accelerometer data from three nearby stations (NC.KCT, BK.PETL, and BK.BJES). The Green's function were calculated using the GIL7 velocity model (Dreger and Romanowicz, 1994) and the *f-k* integration code from Herrmann (2013) for a sampling frequency of 10 Hz. The HH velocity data (BK.JCC, BK.SIGP, BK.SCOT, BK.PETY, and BK.WEAV) and HN acceleration data (BK.BJES, NC.KCT, and BK.PETL) from the BK and NC networks (see Data and Resources) were instrument corrected and resampled from 100 samples per second to a sample rate of 10 samples per second using the anti-aliasing filter of the Seismic Analysis Code (Goldstein *et al.*, 2003; Goldstein and 9
Snoke, 2005), filtered with an acausal high-pass Butterworth filter at 0.02 Hz to remove low-frequency drift, and then integrated to displacement. The displacement Green's functions had the same high-pass filters applied.

It proved difficult to model the broadband signals since the second event initiates at approximately the time the *S* wave of the offshore event arrives at its hypocentral location, and there is no or at best very little separation of the *S*-wave arrivals from the two sources at many stations. Compounding the modeling challenge is the inherent nonuniqueness of kinematic finite-source inversions as illustrated by Beresnev (2004) owing to the approximations made in describing the kinematic process, and the underdetermined nature of the inversion. To partially overcome this, we apply both slip positivity and smoothing constraints to the model. With this analysis we attempt to develop a rupture model using the NCSS constrained, hypocentral locations for the two events (Table 1). Rupture was allowed to occur along three fault planes. For 2021-OFF, we assume a strike/rake/dip (s/r/d) consistent with the strike of the Mendocino fault (s/r/d = 270°/−180°/90°), a hypocenter at 40.298° N 124.626° W and a depth of 16.5 km. For 2021-ON, we use the hypocenter from the NCSS catalog at 40.380° N, 124.298° W, a depth of 27 km, and the two conjugate fault planes for the best-fit moment tensor from the regional

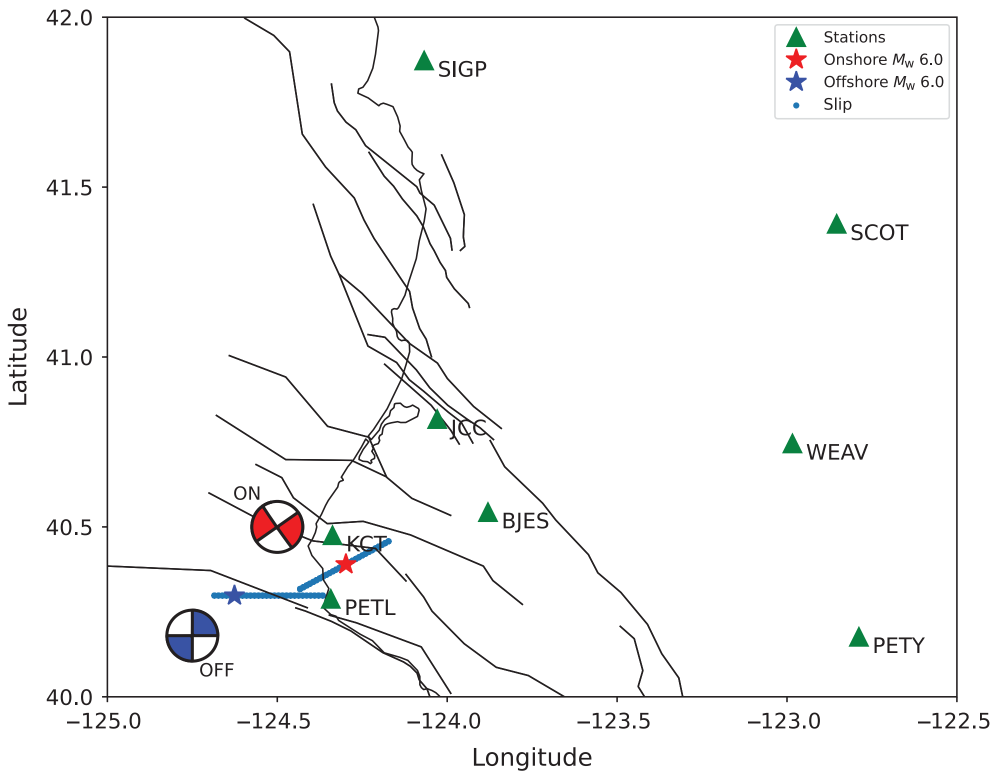

Figure 4. Finite-source analysis for 2021-OFF and 2021-ON. Location map showing the stations used (green triangles) and the mechanisms used for 2021-OFF (blue, OFF) and 2021-ON (red, ON). The extent of the fault planes
28 considered in the inversion is shown as thick blue lines.

moment tensor analysis (northeast: s/r/d = 54.7°/−1.4°/90° and southeast: s/r/d = 145°/−180°/90°). The fit for the northeast-striking plane of 2021-ON was better; therefore, Figure 4 shows only its location and strike and that of the Mendocino fault event, along with the mechanisms and the seismic stations used in the inversion. It is important to recognize that given the station geometry, the complexity of the sources, and the frequency content and nearly synchronous timing of the waves, there is much freedom in setting the s/r/d of the faults. Therefore, we choose to present simple models with vertically dipping planes. This allowed us to test a range of strikes to find a combination that fit both the long- and short-period amplitudes well. The preferred rupture plane for 2021-ON strikes to the northeast, although the fit for this plane (58%) is only slightly better than for the southeast-striking plane (56%).

Another free parameter in the inversion is the interval between the origin-times of 2021-OFF and 2021-ON. Trial and error modeling provided the best fit to the data and found a delay between the two events of approximately 11 seconds. This timing is consistent with the detailed phase picking reported earlier. We conclude that 2021-ON initiates 11 seconds after 2021-OFF and has a fault orientation of s/r/d of 55/-1/90.

Figure 5a shows the slip model for 2021-OFF, which has a primary asperity, with a peak slip of 51.0 cm just to the west of the hypocenter and ruptures slightly downward. A second patch of slip located approximately 10 km to the east along the Mendocino fault, ruptures about 8 s later. The average slip for the model is 12.6 cm. The areas of each of the two slip patches are roughly 5×5 km^2 with the eastern patch slipping less. There is low level, spurious slip in the model in which we have no confidence. The total moment for 2021-OFF is 1.35×10^{18} N · m corresponding to M_w 6.02.

The main patch of slip for 2021-ON on the northeast-striking plane (Fig. 5b) extends upward and northeast from the hypocenter indicating unilateral rupture. The slip patch covers an area of about 12 km vertically by 8 km horizontally and encompasses three substantial subpatches of slip, with maximum and average slip of 45.2 and 14.4 cm, respectively. The slip occurs between 15 and 28 km depth, well below the depth of the subduction interface inferred by relocated intraslab earthquakes in this study and others (Yeck *et al.*, 2023; Shelly *et al.*, 2024; Yoon and Shelly, 2024), indicating that the rupture is within the subducted Gorda plate, most likely the upper mantle. As is the case for 2021-OFF, there is spurious slip imaged in the 2021-ON model in which we have no confidence.

The total moment for 2021-ON is 1.57×10^{18} N · m, corresponding to M_w 6.06. Thus, in this model both events have roughly the same magnitude indicating the event is a doublet. The apparent difference in their recorded amplitudes arises from the fact that 2021-ON ruptured under the continent and therefore much closer to the recording stations. Using the GIL7 velocity model to estimate the *S*-wave travel time from the hypocenter of 2021-OFF to the hypocentral location of 2021-ON gives 8.3 s. This is close to the modeled trigger time of 11 s after the nucleation of 2021-OFF, indicating 2021-ON was likely dynamically triggered.

The event depths are one of the better-constrained elements of the model (Fig. 5a,b). In contrast, constraints on rupture speed are limited by the fact that we model both earthquakes of the doublet in a single process, although they are separated both in time and space. The apparent rupture velocity for 2021-OFF on the Mendocino fault is very low at 1.2 km/s.

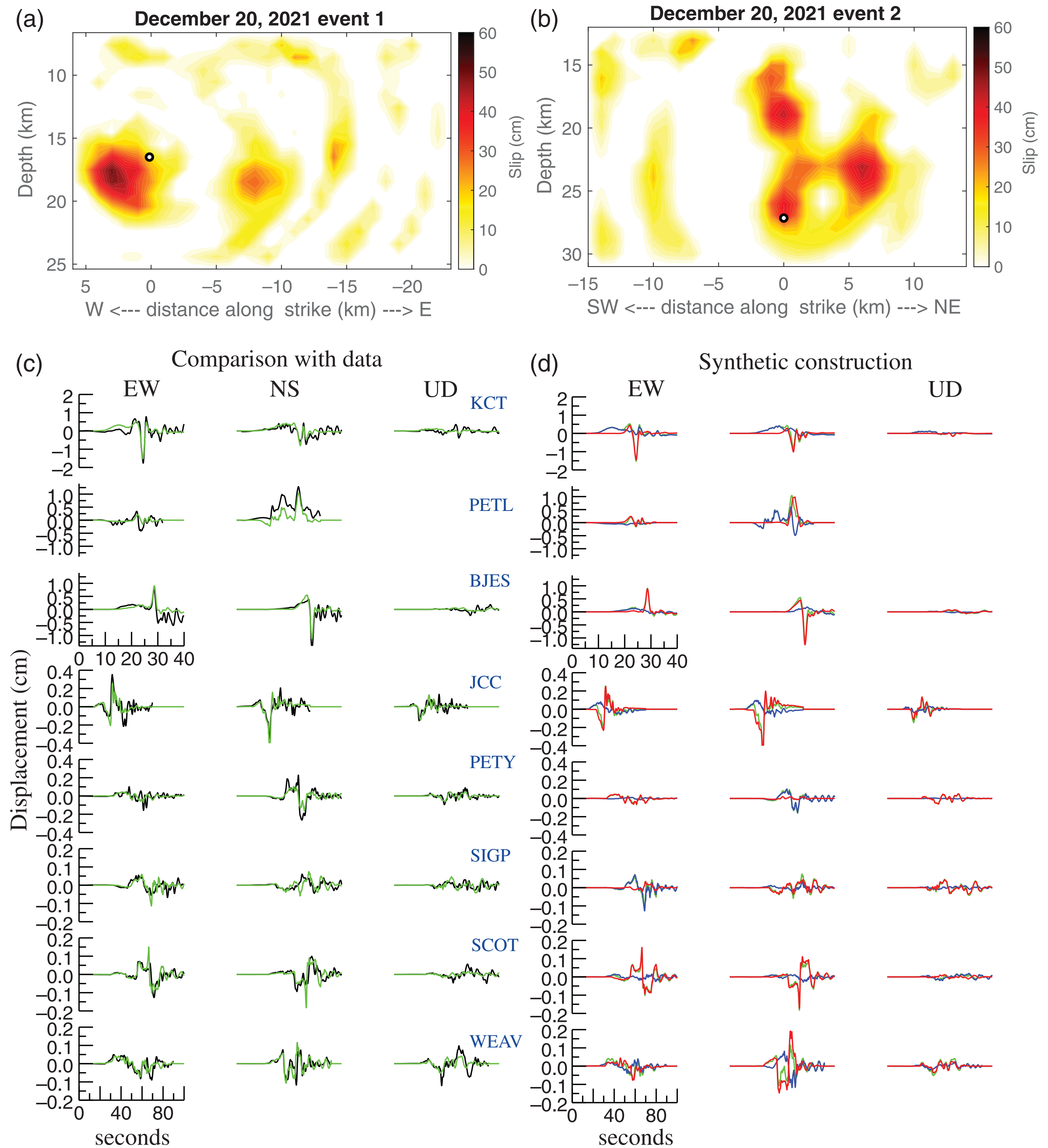

Figure 5. (a) Slip model for 2021-OFF, located offshore along the strike of the Mendocino fault. Strike of the fault is N270°E. (b) Slip model for 2021-ON located onshore 29 km east-northeast of 2021-OFF. Strike of the fault is N55°E. Black circles indicate the hypocenters in the model. (c) Comparison of the fit of the model (green) to data (black). (d) The complete synthetics (green) are constructed by summing the synthetics from 2021-OFF (blue) and 2021-ON (red).

This may be due to serpentinization of the fault zone inferred by Materna *et al.* (2018) from the occurrence of characteristic repeating earthquakes. On the other hand, the rupture velocity for 2021-ON is more typical at 2.5 km/s, which corresponds to 74% of the shear-wave velocity of model GIL7 at the depth for which the principle slip occurs.

Overall, the fit of the composite source model to the broadband data is good (Fig. 5c). The construction of the synthetic displacement waveforms (Fig. 5d) is dominated by the onshore event, 2021-ON (red) because this source is much closer to most of the stations. Three stations, BK.PETL, BK.PETY, and BK.SIGP, exhibit the greatest contribution from the offshore earthquake, 2021-OFF (blue). BK.WEAV also has a significant contribution from 2021-OFF but there is more interference between arrivals from both sources. BK.PETL is the station closest to 2021-OFF, and the two subevents of 2021-OFF are clearly apparent on its north–south component. This station has nearly equal contributions from both members of the doublet. Interestingly, the other two stations, BK.PETY and BK.SIGP, are among the most distant stations (Fig. 4), which would give greater temporal separation of the wavefields radiated from the two respective sources. These stations are also located at directions close to nodal *SH* radiation from 2021-ON and close to maximum *SH* radiation from 2021-OFF, which can be seen on their north–south and east–west components, respectively. The overall fit is good, but it is important to remember that confidence in the details of these slip models is not high due to the complexity of the doublet and relatively sparse station coverage.

Seismicity of the December 2021 sequence

The aftershock activity following the initial 20 December 2021 event, 2021-OFF, was an important indicator that it was not a typical, single mainshock along the Mendocino fault, a common source of northern California seismicity. Rather than just a relatively simple distribution of aftershocks along the fault, an appreciable cluster of earthquakes developed to the northeast of 2021-OFF, beneath the sparsely populated onshore region of the MTJ (Fig. 1, orange dots).

The slip in the finite-source model for 2021-OFF occurred below a depth of 15 km in two patches on the easternmost section of the Mendocino fault, where the fault descends beneath the overriding NAP. All the slip occurred below the megathrust and the wedge of the NAP above it. This interface lies just above the pale gray band of seismicity on the lower plots in Figure 6a,b. The strike-slip mechanism of 2021-OFF is typical for earthquakes along the Mendocino fault, and consistent with the right lateral movement between the Gorda and PPs (Materna *et al.*, 2018). The aftershocks along the fault are also fairly typical for Mendocino fault events (Fig. 6a). In map view, they form a line about 25 km long reaching almost to the coast (Fig. 6a, top). Viewed from roughly south (Fig. 6a, bottom), their locations are consistent with the finite-fault results shown in Figures 5a and 6a, bottom (green), mostly bracketing the areas of rupture and tracking the depth of energy release. The right-lateral, strike-slip mechanisms of the aftershocks are also typical of Mendocino fault seismicity.

The second member of the doublet, 2021-ON, initiated 11 s after 2021-OFF and about 29 km to northeast (Fig. 1). This event is well north of the southern edge of the descending Gorda plate and also below the subduction interface. This places 2021-ON entirely within the Gorda plate, most likely rupturing the upper mantle (Yeck *et al.*, 2023; Yoon and Shelly, 2024). Its strike-slip mechanism is a response to north–south compression and is consistent with the mechanisms of earthquakes rupturing offshore faults in the Gorda basin (e.g., Guilhem and Dreger, 2011) and west of the corner of the PP (McPherson, 1989; Cockerham *et al.*, 1992; Smith 10
et al., 1993; Wada *et al.*, 2010).

In map view, the aftershocks form an amorphous cluster, with 2021-ON near the south end of the cloud (Figs. 1, 6b). The aftershocks are broadly distributed in area and depth, possibly on some of the many fractures present in the subducting plate (Gullick *et al.*, 1997, 2001). No clear lineations are present that might suggest a preference for the rupture of the northeast or southeast planes of the mechanism, as discussed in the section on the finite-source inversion, nor an obvious outline of the rupturing fault. Thus, the determination of the fault plane is limited by the uncertainties in modeling the waveforms. However, it is apparent that the fault responsible for 2021-ON is entirely within the Gorda plate and below the interface of the megathrust and results from north–south directed compression (Yeck *et al.*, 2023; Yoon and Shelly, 2024, this study).

20 DECEMBER 2022 EARTHQUAKE SEQUENCE

The 20 December 2022 earthquake initiated at 10:34:24.77 UTC (02:34:24.77 PST) offshore of False Cape, well north of the Mendocino fault (Fig. 1, Table 1). This earthquake, with M_w 6.4, and its aftershocks were more significant than the 2021 events in terms of damage and their effects on the local population.

December 2022 finite-source inversion

The hypocenter of the 20 December 2022 Ferndale earthquake (2022-MS) is approximately 18 km west-northwest of the onshore event of 20 December 2021 (2021-ON). The distribution of recorded strong ground motion and reported damage indicates directivity to the northeast. Because this event was larger than those of 20 December 2021, it was better recorded seismically, and also registered static ground deformation from GNSS and InSAR systems, although an event of this magnitude is close to the latter's noise level.

The finite-source model reported by the USGS (see Data and Resources) has relatively low levels of slip, peaking at about 0.5 m with a smooth distribution over an area of approximately 20×20 km^2. The slip is located up-dip and to the northeast of the hypocenter, suggesting that the earthquake initiated in the Gorda plate and ruptured through the subduction interface into the NAP, although all the mapped faults in the NAP trend at an oblique angle to the hypothesized rupture plane (Fig. 7) and the orientation of the stress tensor in the NAP is distinctly different from that in the Gorda plate (McPherson, 1989; Smith *et al.*, 1993). The seismic waveform data used in the USGS finite-source analysis appear to have been low-pass filtered at approximately 0.3 Hz.

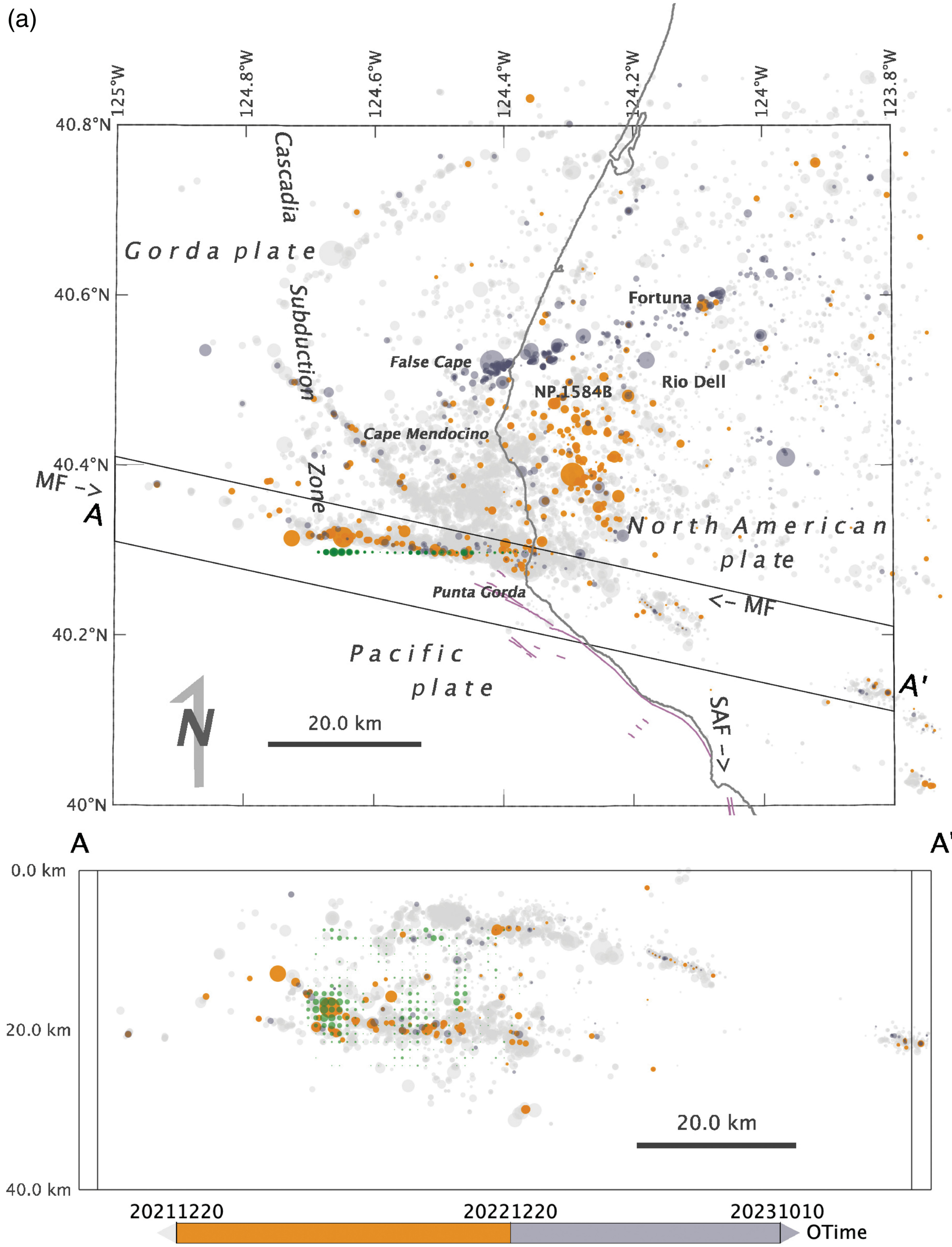

Figure 6. Plot of NLL-SC-relocated seismicity from the Northern California Seismic System (NCSS) catalog (see Data and Resources). Seismicity from 1982 to 20 December 2021 is pale gray, from 20 December 2021 to 19 December 2022 is orange, and from 19 December 2022 to 10 October 2023 is dark gray. The top of the Gorda plate (the megathrust) lies just above the upper, pale gray band of seismicity on the profile plots. MF, Mendocino fault; SAF, San Andreas fault. (a) Green dots indicate the finite-source model for 2021-OFF, with the dot size indicating the estimate of slip; note that the model strike (270°) is not quite that of the Mendocino fault, so the source model does not lie exactly on top of the Mendocino fault seismicity. Top: view from above. Bottom: view from azimuth 192° from north showing only events along the MF within the black lines in the top plot. (b) Finite-source model for 2021-ON. Green dots indicate the rupture estimate from the finite-source model with dot size scaling with the slip estimate. Top: view from above. Bottom: section view from azimuth 144° from the north showing only events within the black rectangle in the top plot. (*Continued*)

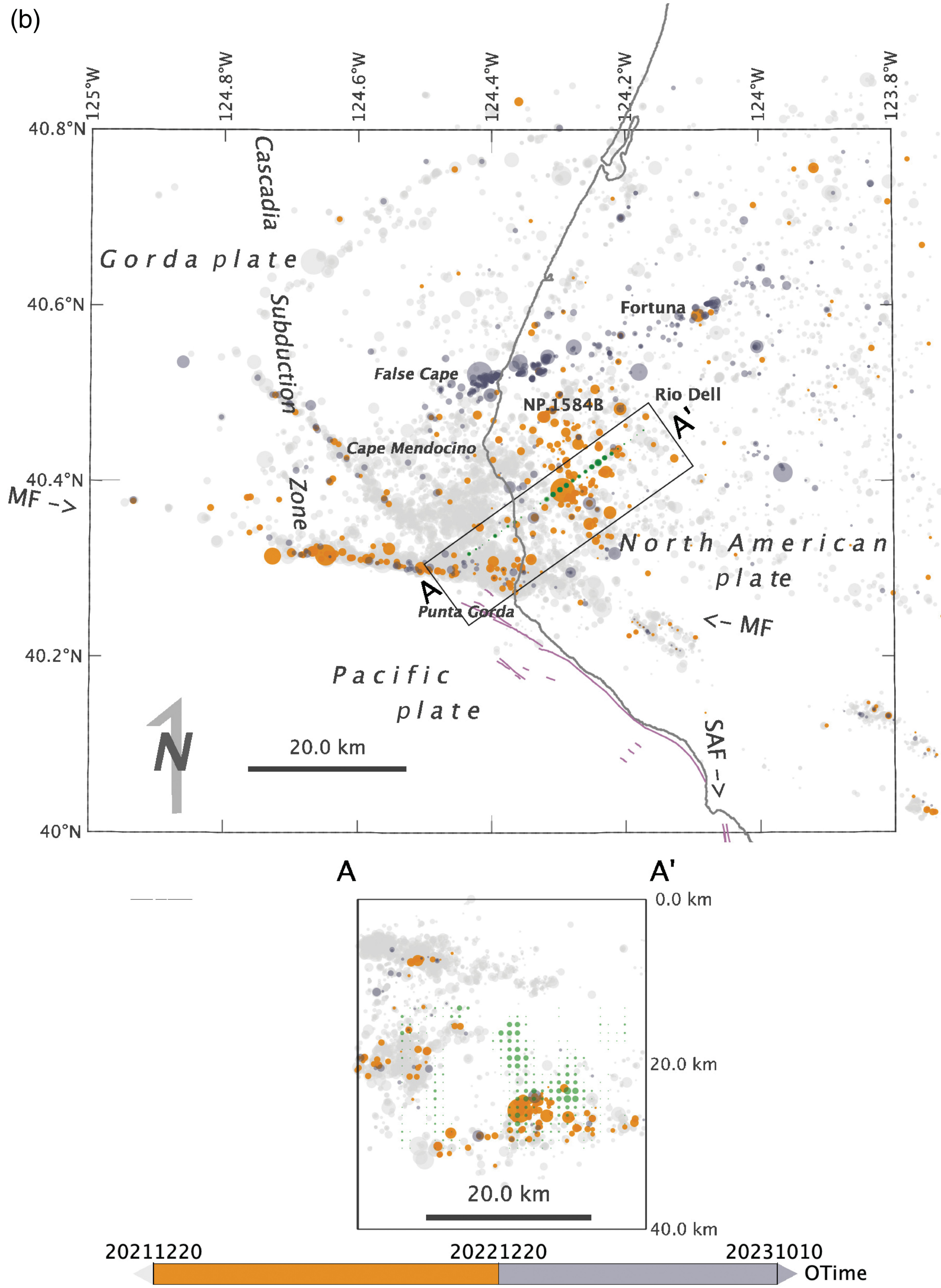

Figure 6. Continued

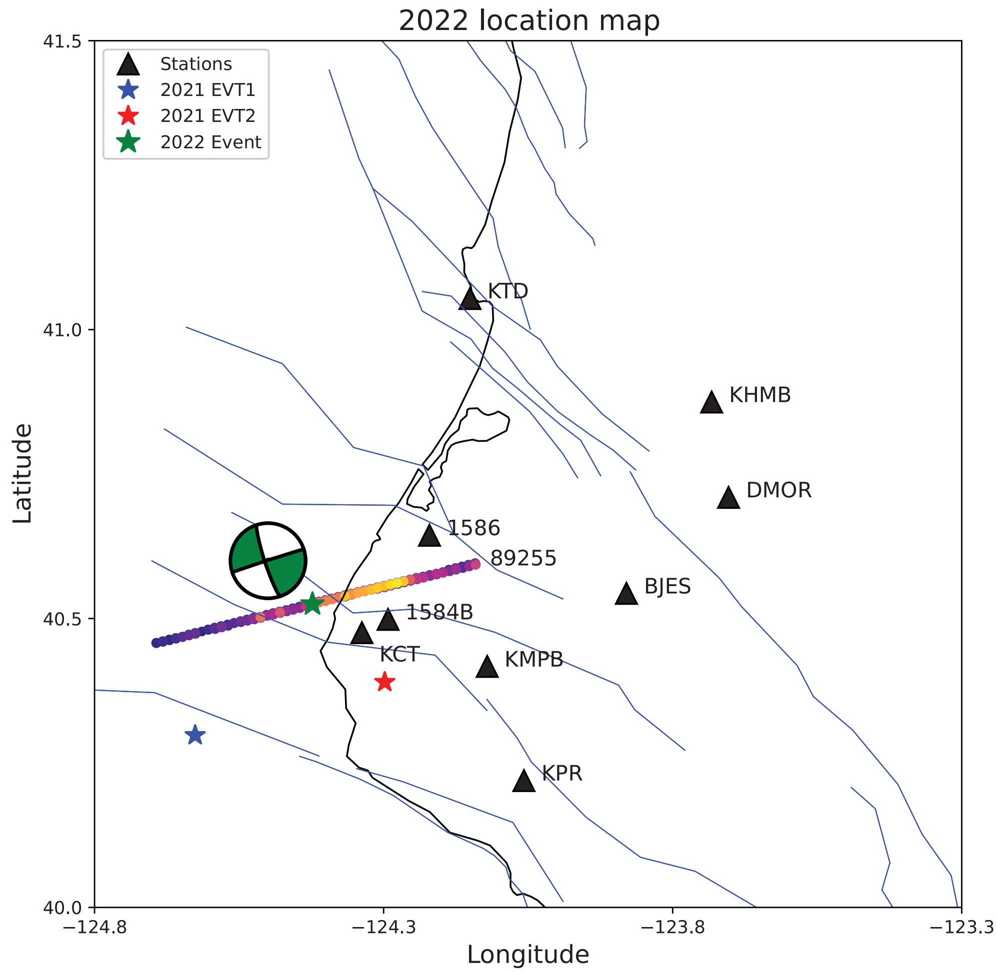

Figure 7. Location of the 2022 M_w 6.4 Ferndale earthquake (green star). The Berkeley Seismology Laboratory (BSL) moment tensor solution is shown with the locations of the 2021 M_w 6.0 events (blue star: 2021-OFF, red star: 2021-ON). Stations from the BK, CE, NC, and NP networks (see Data and Resources) used for the finite-fault inversion are indicated with black triangles. The extent of the finite-source model is also plotted. The main slip (warmer colors) is located east-northeast of the epicenter. Narrow pale lines indicate faults in the North American plate (NAP).

The BSL's regional moment tensor solution (see Data and Resources, Dreger, 2018) finds a scalar moment of 5.05×10^{18} N · m (M_w 6.40) at a depth of 24 km with s/r/d = 252°/7°/89°. For our finite-source analysis, we assume the strike and dip from the moment tensor and allow for variable rake angle over six time windows using the Hartzell and Heaton (1983) linear inversion method as implemented by Kaverina *et al.* (2002). Instrument-corrected data from 10 nearby three-component stations (Fig. 7) from the BK, CE, NC, and NP networks (see Data and Resources) were integrated to ground displacement and resampled to 10 Hz. The data were high-pass filtered at 0.02 Hz to remove long-period drift in the records, but no low-pass filter was applied. The GIL7 (Dreger and Romanowicz, 1994) velocity model was used to compute Green's function using the CPS3.0 software from Herrmann (2013) and comparable filters were applied. In addition, static offsets from 24 GNSS sites were also used in the inversion. The processed GNSS data were provided by Jerry Svarc (personal comm., 2023).

The slip inferred from the joint inversion of the seismic waveform and GNSS deformation data indicates that the rupture proceeded predominantly toward the east-northeast (Fig. 8a). The peak slip of approximately 1.51 m took place between 10 and 15 km along the strike to the east-northeast of the hypocenter and 2–5 km below it. This late burst of slip likely also contributed to the high accelerations and exacerbated levels of damage and the perceptions of strong shaking.

In notable contrast to the USGS model with a slip shallower than the hypocenter, the main slip from this earthquake extended to the east from the hypocenter and downward with a predominantly horizontal rupture direction. Rupture extends from depths of 17 km to approximately 24 km, consistent with the moment tensor depth of 24 km for the main moment centroid. The slip is framed by relocated events above the slip patch and below the top of the subducted Gorda plate as inferred from the top of the intraslab seismicity. This interpretation is corroborated by a variety of studies of the location of the megathrust interface in this region (McPherson, 1989; Smith *et al.*, 1993; Beaudoin *et al.*, 1994; Gullick *et al.*, 1997; McCrory *et al.*, 2012; Delph *et al.*, 11
2018; Guo *et al.*, 2018, 2021; Hayes *et al.*, 2018; Gong and McGuire, 2021; Block *et al.*, 2023; Shelly *et al.*, 2024; Yoon 12
and Shelly, 2024). The slip vectors show that the rupture is predominantly left-lateral strike-slip with minor amounts of dip slip. The total moment inferred from the model is 6.05×10^{18} N · m, corresponding to M_w 6.45, slightly larger than the moment tensor solution. Some spurious, relatively low-amplitude slip, in which we have no confidence, is caused by the skewed coverage of stations used for the inversion. This effect also likely elevates the estimate of the total scalar moment slightly.

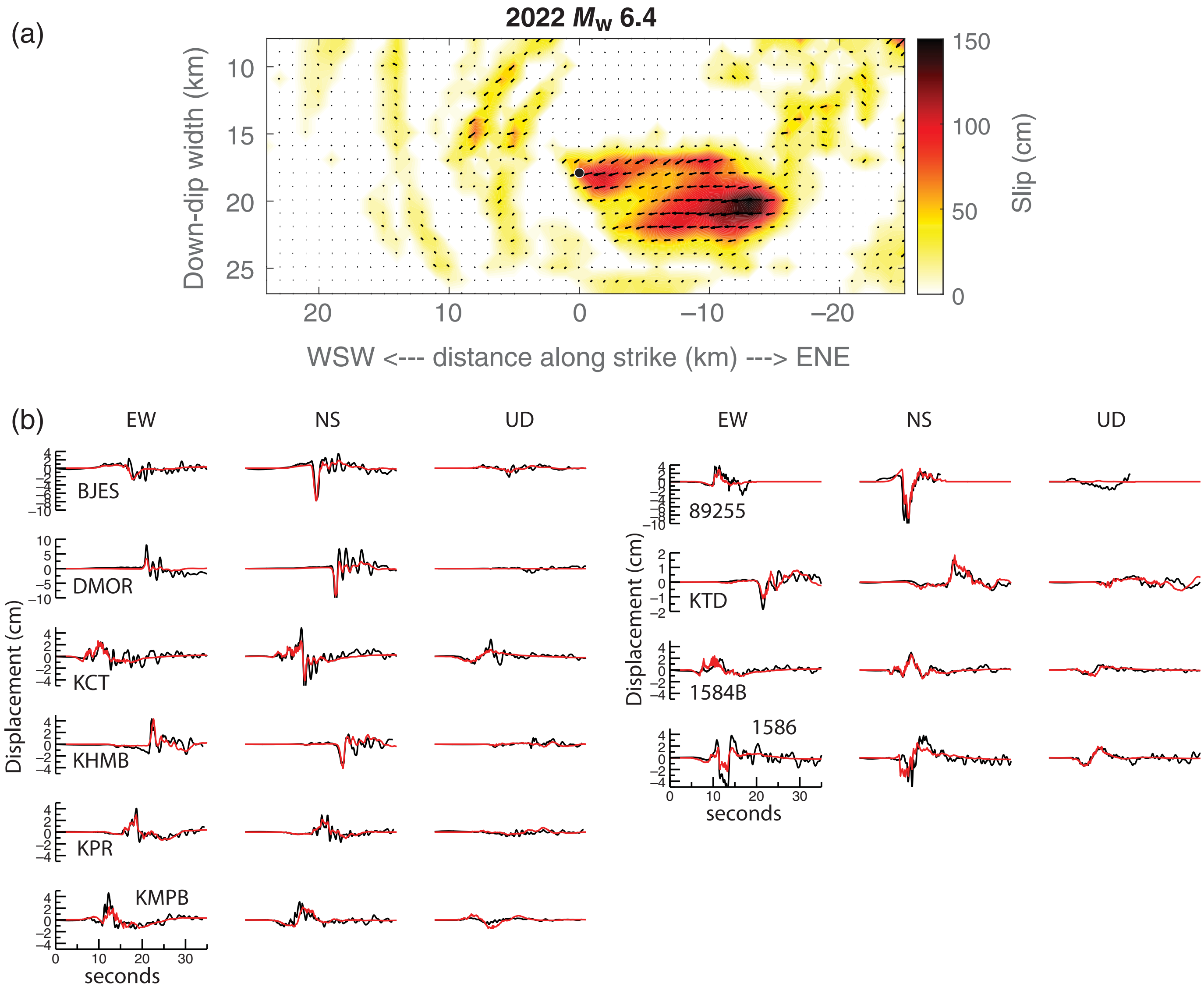

Figure 8. (a) View from the south-southeast of the slip distribution for the 2022 20 December M_w 6.4 Ferndale earthquake determined from joint inversion of seismic waveforms and the Global Navigation Satellite System (GNSS) static deformation data. The hypocenter is shown as a black circle. The arrows show the direction of slip of the side of the fault that is on the page (left lateral). (b) Comparison of observed (black) and synthetic (red) displacement seismograms for the 2022-MS.

The fit to the data is good (Fig. 8b). Three stations, 89255, BJES, and DMOR, are located east of the rupture in the direction of rupture propagation. The waveforms at these stations, which fit the model well, show pulses typical of rupture directivity with very short durations and large amplitudes. Stations 1584B and KCT are located perpendicular to the main rupture. Their waveforms exhibit pulses with longer duration and higher complexity, stemming from the two subevents within the main rupture patch (Fig. 8b).

The fits to the GNSS data (Fig. 9) are good at the more distant stations; however, at the closest stations, P161 (near seismic station 1586), P159 (near seismic station 1584B), and P160, they are relatively poor. P161 is underestimated by about a factor of 2, and P159 and P160 are overestimated. However, the fits to the seismic data at 1586 and 1584B, near P159 and P160 are good. The magnitudes of the synthetic GNSS displacements at these three sites are comparable, which is expected considering they are similar distances from the main slip patch. The asymmetry of P161 versus P159 and P160 might be accounted for by a northwestward dip of the fault plane meaning the fault would extend toward P161; however, all four moment tensor solutions reported on the USGS website have nearly vertical fault planes. Although the model permitted shallow slip, the inversion does not result in any significant coherent slip above the hypocenter. Another possible explanation for the discrepancy between the deformation and the model at these three stations is shallow slip close to P161 that is not part of the primary rupture. We tested this possibility by allowing the fault model to extend close to the surface and slip to occur outside the time window constrained by the

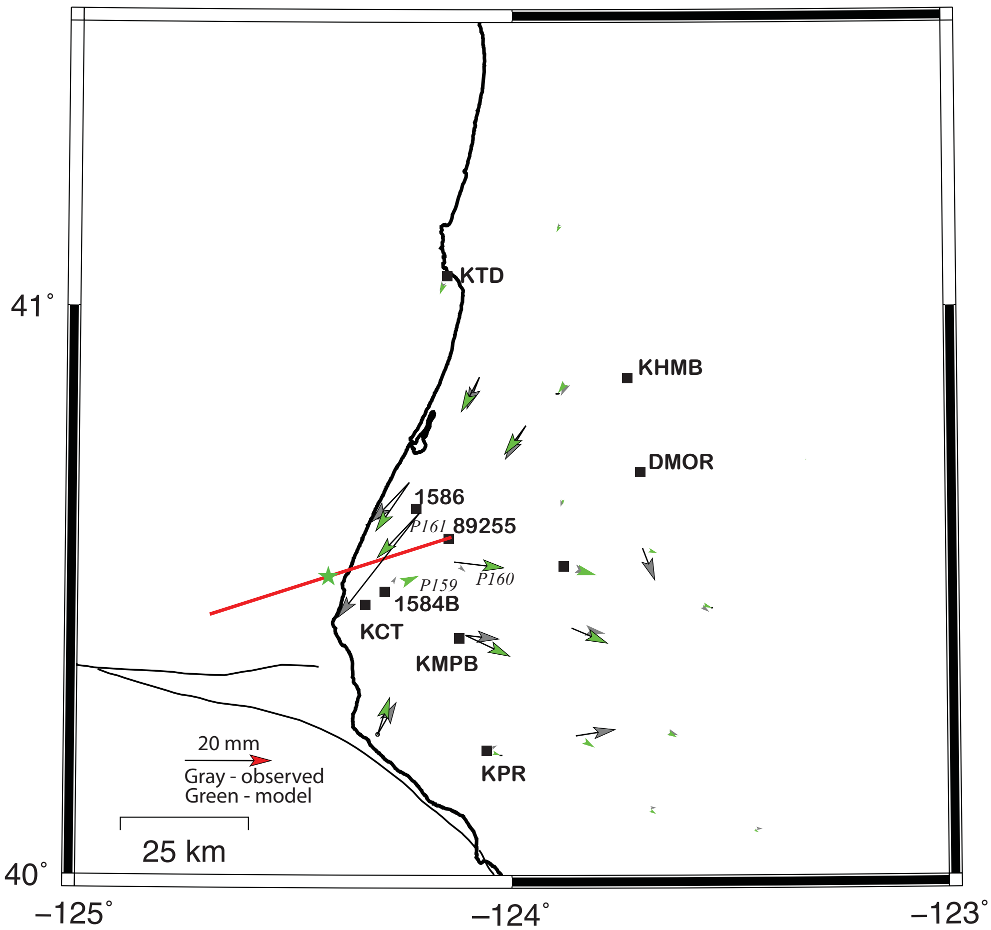

Figure 9. Comparison of observed (gray) and synthetic (green) GNSS displacement. The red rectangle shows the position of the finite-source model. The squares show seismic stations used in the inversion, some of which are collocated with GNSS instruments.

seismic waveform data. With these changes, it is possible to improve the fit to P161, but not sufficiently to warrant accepting the unlikely explanation that this earthquake ruptured through the subduction interface and into the NAP.

2022 shaking and seismicity

The shaking on 20 December 2022 was especially intense in the town of Rio Dell, and to a somewhat lesser degree in the towns of Fortuna and Ferndale. A detailed description of the damage from the shaking was compiled in an report of the Earthquake Engineering Research Institute that compares the damage from the 2022 event with an earlier event from 1975 which occurred on the same fault (Maison, 2023; McPherson *et al.*, 2024). The damage in Rio Dell was significant, with high accelerations recorded (1.44*g*), 30% of chimneys damaged or fallen, cliff failures along the river bluffs, houses knocked off their foundations, and broken water lines. The intense shaking experienced by residents lasted for 15–20 s and was likely due to some combination of four factors: the source as an intraplate oceanic earthquake (Choy and McGarr, 2002; McGarr and Choy, 2002; Chen and McGuire, 2016), the large pulse of slip late in the earthquake, rupture directivity toward the towns, and thick valley fill alluvium at the locations of these three communities (Niazi and Karageorgi, 1992; McLaughlin *et al.*, 2000).

At the shoreline near False Cape, the earthquake also caused earth movements just above the hypocenter (see black triangle, Fig. 1). Figure 10 shows a photograph of the shoreline with the view to the east where an earthflow, block slides, and an uplifted marine terrace are visible. The strong shaking reactivated the block slides and an earthflow, which are indicated by arrows. This produced a region of subsidence (outlined area) in the terrace detected and reported by the landowners (S. Flanagan, personal comm., 2023).

The 2022 mainshock and its aftershocks are displayed in map view and in a depth section perpendicular to the fault in Figure 11. As discussed in the finite-source section for the 2022-MS, the depth of its hypocenter is consistent with slip initiating and rupturing within the oceanic Gorda plate beneath both the NAP and the megathrust interface, which is interpreted as being just above the band of pale gray and blue seismicity in Figure 11b. The aftershocks align along an east-northeast trend, consistent with the moment tensor results and the finite-source model. Starting at the west-southwest end of the rupture, a dense cluster of events near the hypocenter extends along the fault and nicely frames the area of maximum slip (Fig. 11b). We are confident that the slip for 2022-MS is entirely within the Gorda plate, as the depth control derived by comparing the relocated seismicity, the event's aftershocks and the modeled slip is convincing. Its rupture being fully within an oceanic plate contributes to the stronger than expected shaking for an event of its size (Choy and McGarr, 2002; McGarr and Choy, 2002). Interestingly, the aftershocks extend more than 20 km to the east-northeast beyond the earthquake's pulse of maximum slip almost to a point north of the corner of the PP (Fig. 1), where the Gorda slab transitions from north–south compression to downslab tension (Cockerham *et al.*, 1989; McPherson, 1989; Smith *et al.*, 1993). Shelly

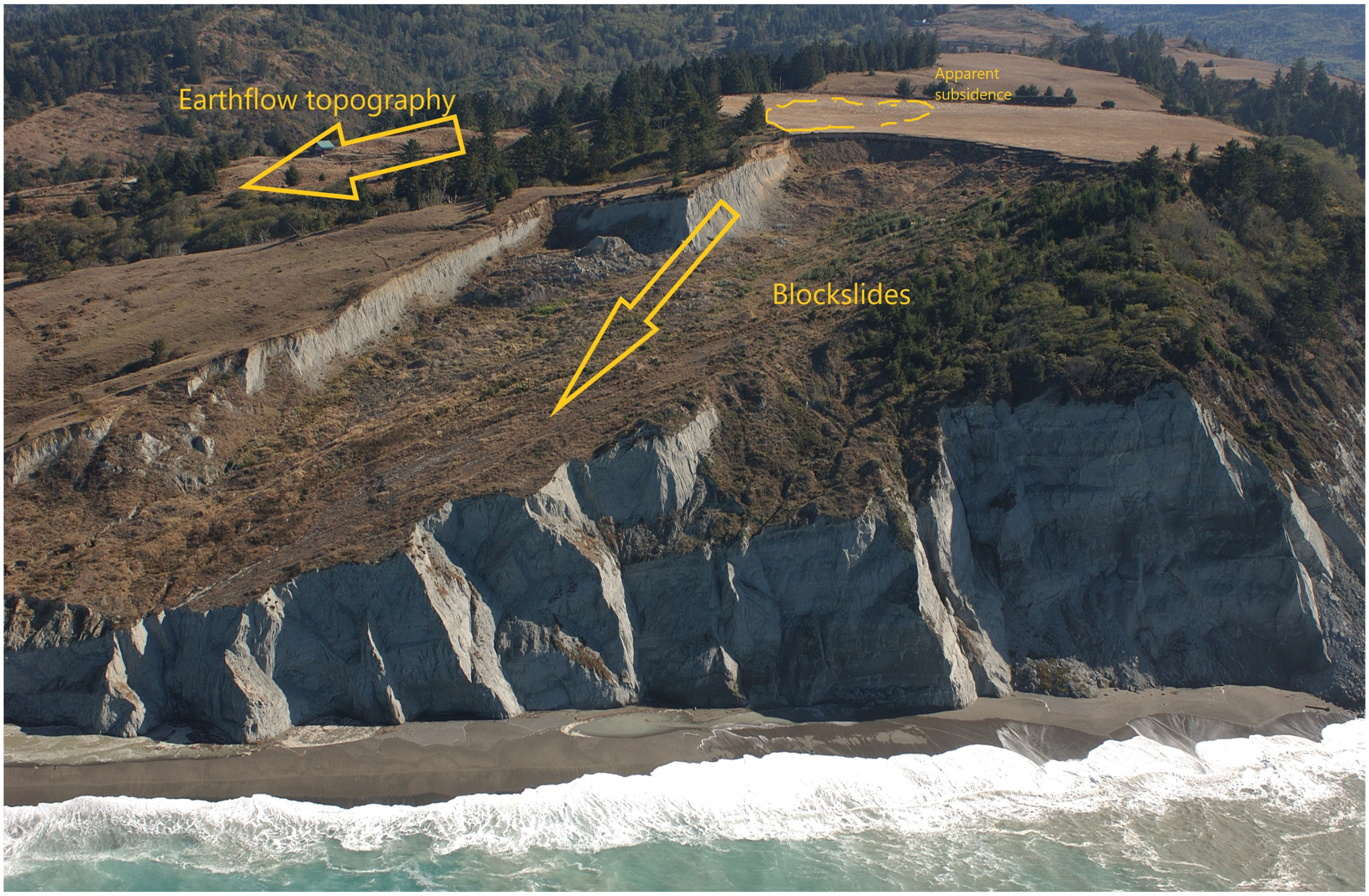

Figure 10. Photograph (see Data and Resources) looking east just south of Flenner Creek, on the coast directly above the 20 December 2022 M 6.4 intraplate earthquake. The movement in the blocks and the reactivation of the earthflow are thought to have caused the warping of the terrace which was noticed by the landowners after the earthquake. The interpretations and annotations are courtesy of Sam Flanagan (personal comm., 2023).

et al. (2024) and Yoon and Shelly (2024) in their figures 1 and 4b, respectively, show focal mechanisms that are predominantly strike slip in the region west of the corner of the PP, whereas those at the east-northeast end of the aftershock sequence have north–south-oriented normal mechanisms. This is evidence that although the 2022 aftershocks extended past the location where the Gorda plate transitions from north–south compression to downslab tension, the 2022-MS rupture appears to have terminated before this transition. This is exactly as predicted by our model of intraslab stress. Overall, quite a few aftershocks were distributed in all directions off the east-northeast end of the trend of the rupture (Fig. 11a), including the largest aftershock, M 5.4, which occurred well below and to the south-southeast of the rupture, 15 km southeast of Rio Dell, California. In addition, many other seismic faults in the region seem to have been activated by the 2022-MS. In the months following its occurrence, seismicity was located on features such as the northwest–southeast-trending offshore lineaments which appeared after the 1992 Cape Mendocino earthquake, in the area of 2021-ON, on the Mendocino fault, along the 1992 rupture plane (Oppenheimer *et al.*, 1993) and in the NAP wedge above and to the northeast of Arcata.

DISCUSSION

The 20 December 2021 doublet proved to be a challenging sequence to unravel. After the sequence began, “the mainshock” on the Mendocino fault was in the NCSS catalog as a single earthquake for more than three weeks before it became clear that two earthquakes had occurred, separated by about 30 km in space and 11 s in time. The first event, 2021-OFF was a typical interplate earthquake on the Mendocino fault: right lateral, vertical strike slip as determined by the fault-plane solution using first motions, and about 25 km offshore. All its aftershocks lie along the Mendocino fault and are interplate events between the Pacific and subducting Gorda plates. The epicenter of the second earthquake, 2021-ON, was onshore, and therefore closer to the monitoring infrastructure, but most of the onsets for nearby stations were hidden in the coda of the first earthquake. Conversely, at more distant stations, the waveforms of the first event were more difficult to distinguish. In the NCSS catalog, this doublet is described as an M 5.7 foreshock followed by an M 6.2 mainshock (Table 1).

Because the second event, 2021-ON was onshore, about 30 km closer to all the near-source instrumentation, its

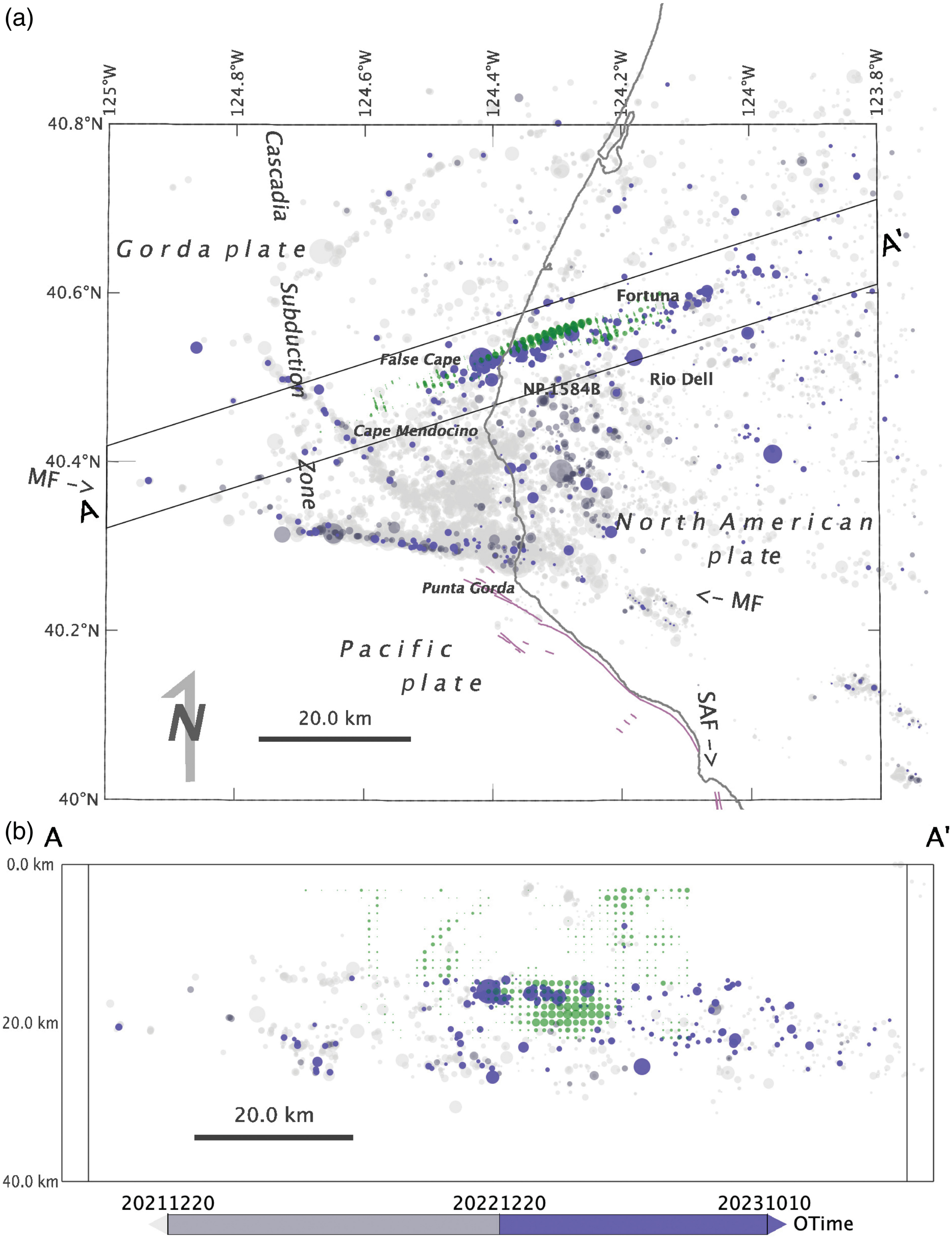

Figure 11. Plot of NLL-SC-relocated seismicity from the NCSS catalog (see Data and Resources). Seismicity from 1982 to 20 December 2021 is pale gray, from 20 December 2021 to 19 December 2022 is dark gray, and from 19 December 2022 to 10 October 2023 is blue. Green dots indicate the finite-source model for 2022-MS, with the dot size indicating the estimate of slip. Top: view from above. Bottom: view from azimuth 162° showing only events within the band between the black lines in the top plot. The top of the Gorda plate (the megathrust) lies just above the band of pale gray and blue seismicity on the lower plot. MF, Mendocino fault; SAF, San Andreas fault.

waveforms and the static displacement it produced are larger in 13 essentially all records. GridMT analysis (Kaverina and Dreger, 2002) clearly finds a reasonable location for the centroid of primary moment release at a depth of 30 km for the second earthquake. Finite-source analysis allowing rupture on faults defined by the Mendocino fault and by the mechanism and location determined for the second earthquake demonstrate that the magnitudes of the two events are approximately equal, with the first having M_w 6.02 and the second having M_w 6.06.

Yeck *et al.* (2023) also determine the rupture processes and slip of the two earthquakes. Our model is derived from continuous waveform data from local accelerometers and regional broadband stations—all onshore, of course—with relatively high signal-to-noise ratio and frequency content up to the Nyquist frequency of the filtered and resampled data just below 5 Hz. In contrast, Yeck *et al.* (2023) invert separate *P*, *S*, and surface-wave data from teleseismic stations, data from 15 nearby accelerometers, and static offsets from 54 regional GNSS stations. Even the largest of the GNSS static offsets close to the epicenter of 2021-ON is only on the order of 5 mm, close to the typical noise level in GNSS data. In addition, the shortest period waveforms in both the teleseismic and accelerometer data used appear to be on the order of 5 s. Thus, some differences in models are to be expected, although in both cases the big challenge is having primarily data from the onshore side of the two earthquakes with the second event closer to all the stations. Yeck *et al.* (2023) modeled this doublet using two pathways. First, using the fault geometries of the mechanisms, they found the best distribution of energy to achieve the observed total *W*-phase moment magnitude for the two events, and determined that the offshore event was slightly larger than the onshore earthquake, with moment magnitudes of M 6.11 and 5.97. Second, their best fit for near-source static surface displacements from GNSS stations gives approximately equal magnitudes for the two events (M 6.0) and depths of 14 km and 25 km. There is substantial agreement in the proposed areas of rupture for each of the events between our model and that of Yeck *et al.* (2023), as well as in moment and aftershock locations. However, there are notable differences. For both events, Yeck *et al.* (2023) estimate a maximum slip on the order of 20–24 cm, whereas the maxima we find (Fig. 5a, b) are more concentrated and have higher slip, 51.0 and 45.2 cm for 2021-OFF and 2021-ON, respectively. Figure 5a, b also exhibits smaller scale details in the amounts of slip at various locations than Yeck *et al.* (2023) show, differences likely due to the longer period data used in their analysis. A second and perhaps more important difference in the two pairs of models are the directions of rupture for 2021-OFF. We estimate that the rupture trends westward and downward from the hypocenter with slip entirely along the Mendocino fault, at 15–20 km well below the top of the Gorda plate. The finite-source model (Fig. 5a) that is nicely bracketed by the aftershocks (Fig. 6a) suggests that slip in 2021-OFF extends below the western wedge of the NAP along the Mendocino fault as it descends beneath North America. In contrast, Yeck *et al.* (2023) model it trending westward and upward. Some of the rupture appears to continue above the Mendocino fault into the westernmost edge of the NAP. Differences in rupture direction are also apparent for 2021-ON. Although Yeck *et al.* (2023) model the rupture trending downward from the hypocenter and to the northeast, our model shows it trending strongly upward and to the northeast. For 2022-ON, both studies agree that the slip patches are entirely contained within the downgoing Gorda slab.

The *S* waves of 2021-OFF apparently trigger 2021-ON after 11 s, 30 km to the east, within the Gorda plate mantle. In our study, the distant response in the Gorda plate is seen as a diffuse cloud of aftershocks. Yeck *et al.* (2023) model this earthquake as a concentrated locus of slip at the hypocenter. Our model, using higher frequency energy from nearby seismic stations, finds that the earthquake ruptures upward, with a burst of energy released about 5 km above hypocenter and a second slip patch to the east (Fig. 5b). The difference between the two models for 2021-ON may be due to the difference in the set of local accelerometers used, but also on the fact that Yeck *et al.* (2023) relied primarily on long-period teleseismic signals. Our joint inversion of the two events used complete waveforms from regional broadband stations, and accelerometers at very short epicentral distances with frequency content between 50 s and 5 Hz to investigate the details of the two nearly synchronous ruptures.

Our confidence that the northeast plane is the correct fault plane for 2021-ON is limited because the variance reduction for this solution is not much better than that of the conjugate plane, 58%–56%, and the locations of the aftershocks are not helpful in determining which fault ruptured, with weak alignment trends favoring the northeast–southwest choice, which matches the fault fabric of the offshore Gorda plate.

The 20 December 2022 M_w 6.4 earthquake was felt strongly by the population in the region and caused damage to buildings and infrastructure. This earthquake began to the north of the 2021 doublet, beginning just offshore of False Cape to the north of Cape Mendocino and rupturing to the east-northeast.

The USGS finite-fault model for 2022-MS (see Data and Resources) describes the rupture as proceeding toward the east-northeast and upward from the hypocenter into the NAP, crossing the subduction interface. In contrast, our finite-fault model for the source begins in the Gorda plate and ruptures east-northeast for some 15 km below the megathrust interface. The strong shaking, damage and high-acceleration amplitudes produced by the earthquake can be explained in part by the rupture directivity. The rupture speed in the model is 3.1 km/s, approximately 78%–90% of the shear-wave velocity of the velocity model at the depths of rupture. Other possible contributing factors include that the fault is rupturing an oceanic plate (Choy and McGarr, 2002; McGarr and Choy, 2002), the late pulse of large slip (~1.5 m) and the thick alluvial deposits on which towns and infrastructure are built.

Aftershocks along the main fault of 2022-MS nicely frame the modeled area of slip (Fig. 11). Similar to what others have found (Shelly *et al.*, 2024; Yoon and Shelly, 2024), they primarily cluster in space and time above the slip patch in the uppermost Gorda crust. However, they exhibit two unusual features: the aftershocks continue in the Gorda plate for more than 20 km along the fault past the end of the modeled rupture to the east-northeast; and in the months following the earthquake, aftershock seismicity was also distributed broadly around the east end of the fault, like buckshot from a shotgun. The focal mechanisms in the dense cluster around the slip patch are consistent with vertical left-lateral sources similar to mainshock (Shelly *et al.*, 2024; Yoon and Shelly, 2024), whereas the easternmost end of the aftershock sequence shifts to north–south-oriented normal faulting. Thus, we infer that while the mainshock began as a response to the north–south compression of the Gorda plate, the aftershocks extend past the corner of the PP into the region dominated by east–west tension. In addition, the 2022-MS seems to have activated many other faults in the region. In the months following, for example, earthquakes appeared along the Mendocino fault and on other features such as the northwest–southeast-trending offshore lineaments of seismicity which appeared after the 1992 Cape Mendocino earthquake, and along the slip plane within the NAP for the 1992 event (Fig. 11). In this way, 2022-MS was similar to the 1992 event, which also triggered aftershock seismicity on many broadly located faults in the region (Oppenheimer *et al.*, 1993).

Similar to 2021-ON, the 2022-MS ruptured within the Gorda plate. Both the mechanism and depth of the modeled rupture and the alignment of the aftershocks are similar to those of the many offshore earthquakes in the Gorda basin (Cockerham *et al.*, 1992; Guilhem and Dreger, 2011) that parallel the trend of the rotated anomalies (Dziak *et al.*, 2001; Wilson, 2002; Chaytor *et al.*, 2004). This supports the interpretation that 2022-MS was an intraplate event within the Gorda plate. It is also evidence that faults within the Gorda plate and therefore the earthquakes they produce maintain the fabric from the Gorda plate as it is subducted. Faults that rupture within the Gorda plate have completely different orientations from those in the overriding NAP.

Although these two sequences are separated in time and space (Yeck *et al.*, 2023; Yoon and Shelly, 2024) and apparently take place on separate faults, we suggest that they are related and help illuminate the ongoing kinematics near the MTJ. 2021-OFF begins the process. This right-lateral event along the easternmost Mendocino fault shifts the Gorda plate under the NAP. 2021-ON, to the east and down slab, is a response to this shift, as a second piece of the Gorda moves incrementally under the NAP. One year later, the large triangular piece of the Gorda plate south of the 2022 aftershock sequence as modeled by Shelly *et al.* (2024) was also allowed to move incrementally under North America, possibly invoking a response in this triangular region on the megathrust above (Shelly *et al.*, 2024). In this way, the December earthquake sequences of 2021 and 2022 are similar to other chains of earthquakes that propagate over time and space outward from the stress concentration at the corner of the PP into the Gorda basin (McPherson *et al.*, 2019).

CONCLUSIONS

The events of the 20 December 2021 doublet provided a challenge in unraveling the overlapping waveforms of the two earthquakes separated by 30 km that were 11 s apart. Careful analysis indicated that the first event of the 2021 sequence occurred offshore along the Mendocino fault because it descends beneath the wedge of the NAP. The *S* waves of this first earthquake, 2021-OFF, triggered a second event. Although this second earthquake, 2021-ON, occurred onshore, beneath the North American continent (and plate), its rupture lies below the subduction interface, within the Gorda plate down-dip and to the east of 2021-OFF. Using finite-source analysis allowing rupture on planes defined by the Mendocino fault and the moment tensor describing 2021-ON, we determined magnitudes for these two earthquakes, estimated to be M_w 6.02 for the first event and M_w 6.06 for the second, and their rupture processes.

The 20 December 2022 M_w 6.4 earthquake occurred in the early morning hours and awakened most people with unusually strong shaking which lasted 15–20 s. We processed broadband data and continuous Global Positioning System data and found 14
that the hypocenter occurred just offshore under the False Cape entirely within the Gorda plate and ruptured to the east-northeast for some 20 km. A cluster of aftershocks in space and time near the hypocenter nicely frames the region of slip. The strong shaking as recorded by accelerometers in the most damaged town of Rio Dell and the damage to structures had a variety of exacerbating causes: unilateral rupture to the east-northeast with directivity pulses toward the towns, enhanced by a strong slip pulse late in the rupture; strong shaking on thick alluvial sediments in the valleys; and the energetic rupture which took place in oceanic crust and upper mantle (Choy and McGarr, 2002; McGarr and Choy, 2002). The 2022 event is a large repeating earthquake, which occurred on a patch of fault that ruptured 47 yr earlier in the 7 June 1975 Rio Dell earthquake (McPherson *et al.*, 2023, 2024). The 2022 earthquake, more so than the 2021 doublet earthquakes, activated faults throughout the MTJ region, producing widely distributed aftershocks. As is apparent in Figures 1 and 11, in the 10 months following the event, earthquakes occurred not only along the rupturing fault, but also along the Mendocino fault at Gorda depths and in the wedge of the NAP above it, as well as along seismic features trending northwest from Punta Gorda that appeared after the 1992 M 7.2 Cape Mendocino event (McPherson, 2024). The east-northeast aftershock zone of the 2022 event extends through the transition

zone separating the offshore region of north–south directed compression from the region of east–west downslab tension.

Our findings for both sequences agree with other analyses (Yeck *et al.*, 2023; Shelly *et al.*, 2024; Yoon and Shelly, 2024) as to the mechanisms and initial hypocenter depths. Although our results show that 2021-OFF occurred entirely along the Mendocino fault and is framed by aftershocks, Yeck *et al.* (2023) has slip extending upward above the Mendocino fault, close to the surface near the subduction front, into a region otherwise devoid of seismicity. We conclude that slip for all the events occurred well below the subduction interface, with no convincing evidence supporting shallower slip. In particular, the rupture of the December 2022 event is entirely within the subducted Gorda plate, in agreement with Shelly *et al.* (2024). It is interesting that the models we present, derived from the inversion of relatively high frequency (0.02–5 Hz) local and regional seismic data as well as GNSS offsets, exhibit both more detailed rupture patterns and higher peak levels of slip than the models of Yeck *et al.* (2023) for the 2021 doublet events. The observation that earthquakes near the MTJ can activate nearby features over different time scales is a complication for analyses of events in this region (Oppenheimer *et al.*, 1993; McPherson, 2024, this article).

DATA AND RESOURCES

Seismic data used in this study are from permanent stations in the region operated as the Northern California Seismic System (NCSS), part of the California Integrated Seismic Network. Waveform data can be obtained from the Northern California Earthquake Data Center (NCEDC) at www.ncedc.org (last accessed January 2024; Northern California Earthquake Data Center [NCEDC], 2014, doi: 10.7932/NCEDC). Operators of seismic stations in the NCSS include the Berkeley Seismology Laboratory (BSL) at the University of California Berkeley operating the Berkeley Digital Seismic Network (BDSN, 2014, network code BK, doi: 10.7932/BDSN), the Bay Area Earthquake Monitoring Project of the U.S. Geological Survey (USGS; EMP, network code NC, doi: 10.7914/SN/NC), the California Geological Survey (CGS) of the State of California (CGS, network code CE), and the National Strong Motion Program (NSMP) of the USGS (network code NP, doi: 10.7914/SN/NP). Geodetic data used in this study are from the Global Navigation Satellite System (GNSS) stations operated by the
15 BSL (BARD, 2014, doi: 10.7932/BARD), the USGS, and UNAVCO (https://www.unavco.org/), and are available from the NCEDC at www.ncedc.org (last accessed January 2024; NCEDC, 2014, doi: 10.7932/NCEDC) and from UNAVCO available at www.unavco.org (last accessed January 2024). The earthquake catalog locations and phase arrival times from the NCSS were used for relocation. The NCSS catalog is hosted at the NCEDC (doi: 10.7932/NCEDC). It can be searched using ncedc.org/ncedc/catalog-search.html (last accessed February 2024) and selecting "NCSS Catalog" from the dropdown menu. Moment tensor solutions from the Berkeley Seismology Lab may be retrieved from the NCEDC (doi: 10.7932/NCEDC) using ncedc.org/ncedc/catalog-search.html (last accessed February 2024) and selecting "Mechanism Catalog" from the dropdown menu. Solutions with waveform fits may also be found at https://www.ncedc.org/mt/ (last accessed February 2024). Figure 1 includes topography and bathymetry from https://www.ncei.noaa.gov/maps/bathymetry/ (last accessed September 2024). The photograph in Figure 10 is from the California Coastal Records Project. It may be found at https://www.cacoast.org/201301638 (last accessed September 2024, Copyright 2002–2024 Kenneth and Gabrielle Adelman, California Coastal Records Project, www. 16
californiacoastline.org). Ground-motion parameters for these earthquakes and others are available at the Center for Engineering Strong Motion Data operated by the CGS at https://www.strongmotioncenter.org (last accessed January 2024). For YouTube video of the collapse of the Scotia Bluffs, see https://www.youtube.com/shorts/uSEViIgvfvI (last accessed January 2024). For YouTube video of the landslide north of False Cape, see https://www.youtube.com/watch?v=thStgCrNVRc (last accessed June 2024). Among other information on earthquakes, the USGS provides finite-fault models for large events such as this 2022-MS, available at https://earthquake.usgs.gov/earthquakes/eventpage/nc73821036/finite-fault (last accessed September 2023). Both the 2021 and 2022 event sequences triggered ShakeAlert are available at https://earthquake.usgs.gov/earthquakes/eventpage/nc73666231/shake-alert and https://earthquake.usgs.gov/earthquakes/eventpage/nc73821036/shake-alert (both last accessed May 2024). The Petrolia earthquake was available at https://www.usgs.gov/programs/earthquake-hazards/news/m62-petrolia-earthquake-december-20-2021-was-really-two (last accessed September 2024). The supplemental material for this article includes a description of the procedures used for NLL-SSST-Coherence (NLL-SC) relocation of the NCSS event catalog, as well as the parameters used for the processing in this study and the catalog of relocated hypocenters (Text S1). The NLL-SC relocated catalog is provided in File S1 and an animated, 3D visualization of the relocations in Movie S1.

DECLARATION OF COMPETING INTERESTS

The authors acknowledge that there are no conflicts of interest recorded.

ACKNOWLEDGMENTS

The authors very much appreciate the effort of the two reviewers, and Associate Editor Shengji Wei, whose comments have contributed to improving this article. Producing earthquake information rapidly after events such as the 2021 and 2022 earthquakes is a collective effort, often entailing exchange of data and enriched by intense discussions. The authors thank Jerry Svarc, Jay Patton, Kathryn Materna, and Andy Barbour for interacting with them. The authors also thank many people in the area, who told them what they experienced in the earthquake, and hope that they are recovering well. None of their work would have been possible without the data from the regional seismic and geodetic stations in the region (BK, NC, CE, NP, BARD, and UNAVCO). The authors are grateful to those who operate and maintain the systems and collect the data. The funds to support these activities and for the expansion of the networks are provided by the California Office of Emergency Services, the U.S. Geological Survey (USGS), the University of California Berkeley, and the National Atmospheric and Space Administration (NASA). The authors very much appreciate the agencies funding earthquake monitoring as well as the operation and maintenance of the seismic and geodetic networks in the region, including the recent improvements.

REFERENCES

Atkinson, G. M., and D. J. Wald (2007). "Did You Feel It?" intensity data: A surprisingly good measure of earthquake ground motion, *Seismol. Res. Lett.* **78,** 362–368.

Atwater, T. (1970). Implications of plate tectonics for the Cenozoic tectonic evolution of western North America, *Geol. Soc. Am. Bull.* **81,** 3513–3536.

Atwater, T., and J. Mudie (1968). Block faulting on the Gorda Rise, *Science* **159,** 729–731.

Bakun, W. H. (2000). Seismicity of California's North Coast, *Bull. Seismol. Soc. Am.* **90,** 797–812.

BARD (2014). Bay Area regional deformation network, *UC Berkeley Seismological Laboratory*, Dataset, doi: 10.7932/BARD.

BDSN (2014). Berkeley digital seismic network, *UC Berkeley Seismological Laboratory*, Dataset, doi: 10.7932/BDSN.

Beaudoin, B. C., M. Magee, and H. Benz (1994). Crustal velocity structure north of the Mendocino Triple Junction, *Geophys. Res. Lett.* **21,** 2319–2322, doi: 10.1029/94GL02154.

Beeson, J. W., S. Y. Johnson, and C. Goldfinger (2017). The transtensional offshore portion of the northern San Andreas fault: Fault zone geometry, late-Pleistocene to Holocene sediment deposition, shallow deformation patterns, and asymmetric basin growth, *Geosphere* **13,** 1–34, doi: 10.1130/GES01367.1.

Beresnev, I. A. (2004). Uncertainties in finite-fault slip inversions: To what extent to believe? (A critical review), *Bull. Seismol. Soc. Am.* **93,** 2445–2458.

Bloch, W.,Bostock, M. G., and P. Audet (2023). A Cascadia slab model from receiver functions, *Geochem. Geophys. Geosys.* **24,** e2023GC011088, doi: 10.1029/2023GC011088.

Braunmiller, J., B. Leitner, J. Nabelek, and A. Trehu (1997). Location and source parameters of the 19 June 1994 (Mw=5.0) Offshore Petrolia California earthquake, *Bull. Seismol. Soc. Am.* **87,** no. 1, 272–276.

Carbotte, S. M., B. Boston, S. Han, B. Shuck, J. Beeson, J. P. Canales, H. Tobin, N. Miller, M. Nedimovic, A. Tréhu, *et al.* (2024). Seismic imaging of Cascadia megathrust morphology, *Sci. Adv.* **10,** doi: 10.1126/sciadv.adl3198.

Chaytor, J. D., C. Goldfinger, R. P. Dziak, and C.G. Fox (2004). Active deformation of the Gorda Plate: Constraining deformation models with new geophysical data, *Geology* **32,** 353–356, doi: 10.1130/G20178.2.

Chen, X., and J. J. McGuire, (2016). Measuring earthquake source parameters in the Mendocino triple junction region using a dense OBS array: Implications for fault strength variations, *Earth Planet. Sci. Lett.* **453,** 276–287.

Choy, G. L., and A. McGarr (2002). Strike-slip earthquakes in the oceanic lithosphere: Observations of exceptionally high apparent stress, *Geophys. J. Int.* **150,** 506–523.

Clarke, S. H., and G. A Carver (1992). Late Holocene tectonics and paleoseismicity, southern Cascadia subduction zone, *Science* **225,** 188–192, doi: 10.1126/science.255.5041.188.

Cockerham, R. W. (1984). Evidence for a 180 km long subducted slab beneath northern California, *Bull. Seismol. Soc. Am.* **74,** 569–576.

Cockerham, R. W., S. W. Smith, R. C. McPherson, and S. H. Clarke Jr. (1989). Earthquake epicenter and selected fault plane solutions of Northern California margin, in *California Continental Margin Map Series, Map No. 7B*, H. G. Green and M. P. Kennedy (Editors), California Division of Mines and Geology.

Delph, J. R., A. M. Thomas, and A. Levander (2021). Subcretionary tectonics: Linking variability in the expression of subduction along the Cascadia forearc, *Earth Planet. Sci. Lett.* **556,** 116724, doi: 10.1016/j.epsl.2020.116724.

Dengler, L., G. Carver, and R. McPherson (1992). Sources of north coast seismicity, California *Geology* **45,** 40–53.

Denlinger, R. P. (1992). A model for large scale plastic yield of the Gorda deformation zone, *J. Geophys. Res.* **97,** 15,415–15,423.

Dreger, D. S. (2003). TDMT_INV: Time Domain Seismic Moment Tensor INVersion, in *International Handbook of Earthquake and Engineering Seismology*, Vol. 81B, 1627. 17

Dreger, D. S. (2018). Berkeley seismic moment tensor method, uncertainty analysis, and study of non-double-couple seismic events, in *Moment Tensor Solutions*, S. D'Amico (Editor), Springer International Publishing, 75–92, doi: 10.1007/978-3-319-77359-9. 18

Dreger, D., and B. Romanowicz (1994). Source characteristics of events in the San Francisco Bay Region, *U.S. Geol. Surv. Open-File Rept. 94-176*, 301–309.

Dreger, D. S., M. H. Huang, A. Rodgers, T. Taira, and K. Wooddell (2015). Kinematic finite-source model for the 24 August 2014 South Napa, California earthquake from joint inversion of seismic, GPS and InSAR data, *Seismol. Res. Lett.* **86,** no. 2A, doi: 10.1785/0220140244.

Dziak, R. P., C. G. Fox, A. M. Bobbitt, and C. Goldfinger (2001). Bathymetric map of the Gorda Plate: Structural and geomorphological processes inferred from multibeam surveys, *Mar. Geophys. Res.* **22,** 235–250.

Eaton, J. (1992). Determination of amplitude and duration magnitudes and site residuals from short-period seismographs in northern California, *Bull. Seismol. Soc. Am.* **82,** 533–579, doi: 10.1785/BSSA0820020533.

Emilia, D. A., J. W. Berg, and W. E. Bales (1968). Magnetic anomalies off the northwest coast of the United States, *Geol. Soc. Am. Bull.* **79,** 1053–1062.

Given, D. D., R. M. Allen, A. S. Baltay, P. Bodin, E. S. Cochran, K. Creager, R. M. de Groot, L. S. Gee, E. Hauksson, T. H. Heaton, *et al.* (2018). Revised technical implementation plan for the ShakeAlert system—An earthquake early warning system for the West Coast of the United States, *U.S. Geol. Surv. Open-File Rept. 2018-1155*, 42 pp., doi: 10.3133/ofr20181155.

Goldstein, P., and A. Snoke, (2005). SAC availability for the IRIS Community, *Incorporated Institutions for Seismology Data Management Center Electronic Newsletter*. 19

Goldstein, P., D. Dodge, M. Firpo, and L. Minner (2003). SAC2000: Signal processing and analysis tools for seismologists and engineers, in *Invited contribution to "The IASPEI International Handbook of Earthquake and Engineering Seismology*, W. H. K. Lee, H. Kanamori, P. C. Jennings, and C. Kisslinger (Editors), Academic Press, London, United Kingdom.

Gong, J., and J. J. McGuire (2021). Constraints on the geometry of the subducted Gorda plate from converted phases generated by local earthquakes, *J. Geophys. Res.* **126,** e2020JB019962, doi: 10.1029/2020JB019962.

Guilhem, A., and D. S. Dreger (2011). Rapid detection and characterization of large earthquakes using quasi-finite-source Green's functions in continuous moment tensor inversion, *Geophys. Res. Lett.* **38,** L13318, doi: 10.1029/2011GL047550.

Gullick, S. S., A. S. Melter, T. J. Henstock, and A. Levander (2001). Internal deformation of the southern Gorda plate: Fragmentation of a weak plate near the Mendocino Triple Junction, *Geology* **29,** 691–694.

Gullick, S. S., A. M. Meltzer, and S. H. Clarke Jr. (1998). Seismic structure of the southern Cascadia subduction zone and accretionary prism north of the Mendocino triple junction, *J. Geophys. Res.* **103,** no. B11, 27,207–27,222, doi: 10.1029/98JB02526.

Guo, H., J. J. McGuire, and H. Zhang (2018). Imaging the subducted Gorda plate: Implications for the stress state and brittle-ductile transition of the Cascadia subduction zone, *AGU Fall Meeting Abstracts*, Vol. 2018, T13H–0334.

Guo, H., J. J. McGuire, and H. Zhang (2021). Correlation of porosity variations and rheological transitions on the southern Cascadia megathrust, *Nature Geosci.* **14,** no. 5, 341–348, doi: 10.1038/s41561-021-00740-1.

Hartzell, S. H., and T. H. Heaton (1983). Inversion of strong ground motion and teleseismic waveform data for the fault rupture history of the 1979 imperial valley, California, earthquake, *Bull. Seism. Soc. Am.* **73,** 1553–1583.

Hayes, G. P., G. L. Moore, D. E. Portner, M. Hearne, H. Flamme, M. Furtney, and G.M. Smoczyk (2018). Slab2, a comprehensive subduction zone geometry model, *Science* **362,** 58–61.

Herrmann, R. B. (2013). Computer programs in seismology: An evolving tool for instruction and research, *Seismol. Res. Lett.* **84,** 1081–1088, doi: 10.1785/0220110096.

Hole, J. A., B. C. Beaudoin, and S. L. Klemperer (2000). Vertical extent of the Newborn San Andreas fault at the Mendocino Triple Junction, *Geology* **28,** 1111–1114.

20 Humboldt County Office of Emergency Services (2023). Dec. 15, 2023 Humboldt county earthquake recovery update, available at https://humboldtgov.org/civicalerts.aspx?aid=5385.

Kaverina, A., D. Dreger, and E. Price (2002). The combined inversion of seismic and geodetic data for the source process of the 16 October 1999 M_w7.1 Hector Mine, California, Earthquake, *Bull. Seismol. Soc. Am.* **92,** 1266–1280.

Kelsey, H., and G. Carver (1988). Late Neogene and Quaternary tectonics Associated with the northward growth of the San Andreas Transform fault, northern California, *J. Geophys. Res.* **93,** 4797–4819.

Lomax, A., and P. Henry (2023). Major California faults are smooth across multiple scales at seismogenic depth, *Seismica* **2,** no. 1, doi: 10.26443/seismica.v2i1.324.

Lomax, A., and A. Savvaidis (2022). High-precision earthquake location using source-specific station terms and inter-event waveform similarity, *J. Geophys. Res.* **127,** e2021JB023190, doi: 10.1029/2021JB023190.

21 Maison, B. S. E. (2023). Damage in Rio Dell from Ferndale Earthquakes 20 December 2022 and 1 January 2023, *EERI Learning from Earthquakes, Ferndale Earthquake Clearinghouse*, available at https://learningfromearthquakes.org/2022-12-20-ferndale-ca/.

Materna, K., J. R. Murray, F. Pollitz, and J. R. Patton (2023). Slip deficit rates on southern Cascadia faults resolved with viscoelastic earthquake cycle modeling of geodetic deformation, *Bull. Seismol. Soc. Am.* **113,** no. 6, 2505–2518.

Materna, K., T. Taira, and R. Bürgmann (2018). A seismic transform fault slip at the Mendocino Triple Junction from characteristically repeating earthquakes, *Geophys. Res. Lett.* **45,** 699–707, doi: 10.1002/2017GL075899.

McCrory, P. A., J. L. Blair, F. Waldhauser, and D. H. Oppenheimer (2012). Juan de Fuca slab geometry and its relation to Wadati-Benioff zone seismicity, *J. Geophys. Res.* **117,** no. B9, doi: 10.1029/2012JB009407.

McGarr, A., and G.L. Choy (2002) Earthquakes having high apparent stress in oceanic intraplate lithosphere, in *The Cascadia Subduction Zone and Related Subduction Systems: Seismic Structure, Intraslab Earthquakes and Processes, and Earthquake Hazards*, S. Kirby, K. Wang, and S. Dunlop (Editors), U.S. Geological Survey Open-File Report 02-328, Geological Survey of Canada Open File 4350, 182 pp., available at https://pubs.usgs.gov/of/2002/0328/.

McKenzie, K. A., and K. P. Furlong (2021). Isolating non-subduction-driven tectonic processes in Cascadia, *Geosci. Lett.* **8,** no. 1, 1–12, doi: 10.1186/s40562-021-00181-z.

McLaughlin, R. J., S. D. Ellen, M. C. Blake Jr., A. S. Jayko, W. Irwin, K. R. Aalto, G. A. Carver, S. H. Clarke Jr., J. B. Barnes, J. D. Cecil, *et al.* (2000). Geology of the Cape Mendocino, Eureka, Garberville, and southwestern part of the Hayfork 30 x 60 minute quadrangles and adjacent offshore area, northern California, with digital database, *Miscellaneous Field Studies Map 2336*.

McPherson, R. C. (1989). Seismicity and Focal Mechanisms near Cape Mendocino, northern California: 1974-1984, *Master Thesis*, Humboldt State University, 75 pp.

McPherson, R. C. (2024). Triggering of nearby faults by large earth- 22
quakes near the MTJ, *Northern California Earthquake Hazards Workshop*, 2024.

McPherson, R. C, J. Patton, D. Dreger, L. Dengler, M. Hellweg, and A. Lomax (2024). Offshore Seismic Hazards in Southern Cascadia (Abstract), *Seismol. Res. Lett.* **95,** 1386.

McPherson, R. C., J. Patton, and A. Lomax (2023). SEISMIC DÉJÀ 23
VU IN 2022, *Northern California Earthquake Hazards Workshop*, February 2023.

McPherson, R. C., S. W. Smith, T. B. Williams, J. Patton, and M. Hemphill-Haley (2019) Complicated kinematics in the Southern Cascadia Subduction Zone, *Seismol. Res. Lett.* **90,** no. 2B, 939.

Northern California Earthquake Data Center (NCEDC) (2014). Northern California earthquake data center, *UC Berkeley Seismological Laboratory*, Dataset, doi: 10.7932/NCEDC.

Niazi, M., and E. Karageorgi (1992). Irregular geometry of the Gorda subduction and deep structure of the Eel River Basin determined from teleseismic P delays, *Tectonophysics* **201,** 209–228.

Nuyen, C. P., and D. A. Schmidt (2022). Strain partitioning among forearc faults in southern Cascadia inferred from GNSS, *J. Geophys. Res.* **127,** e2022JB024236, doi: 10.1029/2022JB024236.

Ogle, B. A. (1953). Geology of the Eel River valley area, Humboldt 24
County California, *CDMG Bulletin*, Vol. 164, 128 pp.

Oppenheimer, D., G. Beroza, G. Carver, L. Dengler, J. Eaton, L. Gee, F. Gonzalez, A. Jayko, W. Li, M. Lisowski, *et al.* (1993). The Cape Mendocino, California, earthquakes of April 1992: Subduction at the Triple Junction, *Science* **261,** 433–438.

Pasyanos, M. E., D. S. Dreger, and B. Romanowicz (1996). Towards real-time determination of regional moment tensors, *Bull. Seismol. Soc. Am.* **86,** 1255–1269.

Prentice, C. S., D. J. Merritts, E. C. Beutner, P. Bodin, A. Schill, and J. R. Muller (1999). Northern San Andreas fault near Shelter Cove, California, *Geol. Soc. Am. Bull.* **111,** 512–523.

Raff, A. D., and R. G. Mason (1961). Magnetic survey off West Coast of North America, 40^0 N Latitude to 52^0 N Latitude, *Geol. Soc. Am. Bull.* **72,** 1267–1270.

Richter, C. F. (1935). An instrumental earthquake magnitude scale, *Bull. Seismol. Soc. Am.* **25,** 1–32, doi: 10.1785/BSSA0250010001.

Riddihough, R. P. (1980). Gorda plate motions from magnetic anomaly analysis, *Earth Planet. Sci. Lett.* **51,** 163–170.

Riddihough, R. P. (1984). Recent movements of the Juan de Fuca plate system, *J. Geophys. Res.* **89,** 6980–6994.

Rollins, J. C., and R. S. Stein (2010). Coulomb Stress interactions among M 5.9 earthquakes in the Gorda Deformation Zone and on the Mendocino fault zone, Cascadia Subduction zone, and the northern San Andreas fault, *J. Geophys. Res.* **115,** 6367–6373, doi: 10.1029/2009JB007117.

Shelly, D. R, D. E. Goldberg, K. Z. Materna, R. J. Skoumal, J. L. Hardebeck, C.E. Yoon, W. L. Yeck, and P. S. Earle (2024). Subduction intraslab-interface fault interactions in the 2022 Mw 6.4 Ferndale, California, earthquake sequence, *Sci. Adv.* **10,** eadl1226, doi: 10.1126/sciadv.adl1226.

Silver, E. A. (1969). Late Cenozoic under thrusting of the continental margin off Northernmost California, *Science* **166,** 1265–1266.

Silver, E. A. (1971). Tectonics of the Mendocino triple Junction, *Geol. Soc. Am. Bull.* **82,** 2965–2978.

Smith, S. W., J. S. Knapp, and R. C. McPherson (1993). Seismicity of the Gorda Plate, structure of the continental margin, and an eastward jump of the Mendocino Triple Junction, *J. Geophys. Res.* **98,** 8153–8171.

Tsuruoka, H., H. Kawakatsu, and T. Urabe (2009). Grid MT (grid based realtime estimation of moment tensors) monitoring the long-period seismic wavefield, *Phys. Earth Planet. In.* **175,** 8–16.

Uhrhammer, R. A., M. Hellweg, K. Hutton, P. Lombard, A. W. Walters, E. Hauksson, and D. Oppenheimer (2011). California Integrated Seismic Network (CISN) Local magnitude determination in California and Vicinity, *Bull. Seismol. Soc. Am.* **101,** 2685–2693, doi: 10.1785/0120100106.

Velasco, A, C. Ammon, and T. Lay (1994). Recent large earthquakes near Cape Mendocino and in the Gorda Plate: Broadband source time functions, Fault orientations, and Rupture complexities, *J. Geophys. Res.* **99,** no. B1, 711–728.

Wada, I., S. Mazzotti, and K. Wang (2010). Intraslab stresses in the Cascadia Subduction Zone from inversion of earthquake focal mechanisms, *Bull. Seismol. Soc. Am.* **100,** 2002–2013, doi: 10.1785/0120090349.

Wang, K., J. He, and E. Davis (1997). Transform push, oblique subduction resistance, and intraplate stress of the Juan de Fuca plate, *J. Geophys. Res.* **102,** 661–674.

Wei, M., and J. McGuire (2014). The Mw 6.5 offshore Northern California earthquake of 10 January 2010: Ordinary stress drop on a high-strength fault, *Geophys. Res. Lett.* **41,** 6367–6373, doi: 10.1002/2014GL061043.

Williams, T. B., H. M. Kelsey, and J. T. Freymueller (2006). GPS-derived strain in northwestern California: Termination of the San Andreas fault system and convergence of the Sierra Nevada-Great Valley block contribute to southern Cascadia forearc contraction, *Tectonophysics* **413,** 171–184, doi: 10.1016/j.tecto.2005.10.047.

Wilson, D. S. (1986). A kinematic model for the Gorda Deformation Zone as a diffuse southern boundary of the Juan de Fuca Plate, *J. Geophys. Res.* **91,** 10,259–10,269.

Wilson, D. S. (1989). Deformation of the so-called Gorda Plate, *J. Geophys. Res.* **94,** 3065–3075.

Wilson, D. S. (2002). The Juan de Fuca plate and slab: Isochron struc- 25
ture and Cenozoic plate motions, in *The Cascadia Subduction Zone and Related Subduction Systems: Seismic Structure, Intraslab Earthquakes and Processes, and Earthquake Hazards*, S. Kirby, K. Wang, and S. Dunlop (Editors), U.S. Geological Survey Open-File Report 02-328, Geological Survey of Canada Open File 4350, 182 pp., available at https://pubs.usgs.gov/of/2002/0328/.

Yeck, W. L., D. R. Shelly, K. Z. Materna, D. E. Goldeberg, and P. S. Earle (2023). Dense geophysical observations reveal a triggered, concurrent multi-fault rupture at the Mendocino Triple Junction, *Commun. Earth Environ.* **4,** 94, doi: 10.1038/s43247-023-00752-2.

Yoon, C. E., and D. R. Shelly (2024). Distinct yet adjacent earthquake sequences near the Mendocino Triple Junction: 20 December 2021 Mw 6.1 and 6.0 Petrolia, and 20 December 2022 Mw 6.4 Ferndale, *Seism. Record* **4,** no. 1, 81–92, doi: 10.1785/0320230053.

Manuscript received 6 February 2024

Queries

1. AU: Please provide complete postal service address including university, city, and country for this affiliation.
2. AU: Please indicate if the roman capital M throughout the article should be changed to (1) bold **M** or (2) *M*_w (italic "M" and subscript roman "w").
3. AU: The citation "Atwater *et al.*, 1968" does not have a corresponding Reference entry. There is a "Atwater and Mudie, 1968" in the References, which is not cited in the paper. Please (1) decide whether these refer to the same work and (2) indicate the required changes to the paper and the References.
4. AU: The citation "Gullick *et al.*, 1997" does not have a corresponding Reference entry. There is a "Gullick *et al.*, 1998" in the References, which is not cited in the paper. Please (1) decide whether these refer to the same work and (2) indicate the required changes to the paper and the References.
5. AU: The citation "Gullick, 2001" does not have a corresponding Reference entry. There is a "Gullick et al., 2001" in the References, which is not cited in the paper. Please (1) decide whether these refer to the same work and (2) indicate the required changes to the paper and the References.
6. AU: SSA tries to avoid using a slash in nonmathematical contexts. Please provide alternative wording for "refraction/reflection."
7. AU: Please provide a definition of "NLL-SSST and NLL-SC"; it will be included before the abbreviation.
8. AU: The citation "Hartzell and Heaton (1982)" does not have a corresponding Reference entry. There is a "Hartzell and Heaton (1983)" in the References, which is not cited in the paper. Please (1) decide whether these refer to the same work and (2) indicate the required changes to the paper and the References.
9. AU: As per SSA style, the abbreviation "(SAC)" has been deleted because it is not used again in this article.
10. AU: Although "Cockerham et al., 1992" is cited, there is no corresponding Reference entry. Please provide a Reference entry for this citation, or indicate the citations should be deleted throughout the article.
11. AU: The citation "Delph *et al.*, 2018" does not have a corresponding Reference entry. There is a "Delph *et al.*, 2021" in the References, which is not cited in the paper. Please (1) decide whether these refer to the same work and (2) indicate the required changes to the paper and the References.
12. AU: Although "Block *et al.*, 2023" is cited, there is no corresponding Reference entry. Please provide a Reference entry for this citation, or indicate the citations should be deleted throughout the article.
13. AU: The citation "Kaverina and Dreger, 2002" does not have a corresponding Reference entry. There is a "Kaverina et al., 2002" in the References, which is not cited in the paper. Please (1) decide whether these refer to the same work and (2) indicate the required changes to the paper and the References.
14. AU: Because it was only used once, "GPS" has been replaced with "Global Positioning System"; please provide a corrected definition if needed.
15. AU: Please provide the month and year when you last accessed this website (https://www.unavco.org/) for your article.
16. AU: Please provide the month and year when you last accessed this website (www.californiacoastline.org) for your article.
17. AU: For reference Dreger (2003) Please provide editor name, publisher name location of publisher.
18. AU: For reference Dreger (2018) Please provide location of publisher.
19. AU: For Goldstein, and Snoke, (2005) please provide complete details including doi number, or URL and its last accessed month and year.
20. AU: For Humboldt County Office of Emergency Services (2023) please provide last accessed month and year.
21. AU: For Maison (2023) please provide last accessed month and year.
22. AU: For McPherson (2024) please provide complete details including doi number, or URL and its last accessed month and year.
23. AU: For McPherson et al. (2023) please provide complete details including doi number, or URL and its last accessed month and year.
24. AU: For Ogle (1953) please provide complete details including doi number, or URL and its last accessed month and year.
25. AU: Please provide the month and year when you last accessed this website for your article.
26. AU: Please note that figure legends and axis labels are edited to match the SSA style and to be consistent with the text. Please verify the changes and confirm whether the changes do not affect your intended meaning.
27. AU: Figure 3: SSA style requires the use of scientific notation (e.g., 1 × 10_-3 instead of 1E-3). Please review the edited changes inside Figure 3 to be sure no errors were introduced.
28. AU: Figure 4: please note that "thick green lines" was changed to "thick blue lines" since there was no green line. Kindly check and confirm.
29. AU: SSA tries to avoid using a slash in nonmathematical contexts. Please provide alternative wording for "hypocenter/magnitude."